Retrospect on the Preparation and Application of Perovskite Materials

Junyan Xiang[1,*], Changmo Yao[1], Mei Lu[2], Liheng Guo[1] and Dewang Li[3,4,*]

[1]School of Power Engineering, Chongqing Electric Power College, Chongqing 400053, China

[2]State Grid Chongqing Electric Power Company, Chongqing 400015, China

[3]Tianjin University, Institute of Molecular Aggregation Science, Tianjin 300072, China

[4]Collaborative Innovation Center of Chemical Science and Engineering (Tianjin)

Abstract: In recent years, the diversity of new organic-inorganic hybrid perovskite materials has received extensive attention, for tremendous outstanding properties including large optical absorption coefficients, high carrier transport mobilities, long-range charge-carrier diffusions, low exciton binding energies, adjustable bandgaps, narrow-band bright photoluminescence as well as the compatibility of simple processing techniques. Because of these excellent properties, perovskite materials are widely used in solar cells, light-emitting devices, photodetectors, photocatalysis, etc. Here we reviewed the fundamental structure and properties of perovskite materials, and summarize the diverse preparation methods of perovskites along with the key factors in nucleation and growth control to prepare high-quality bulk crystals or films with less defects and stabilized performances against the external corrosive environments. The applications of perovskite materials accompanied with the relative bulk or interface ameliorations are discussed, and finally the prospects of such materials are expected. Overall, this review demonstrates the prevailing preparation mechanisms, challenges for high-quality perovskite materials and their vital importance in corresponding applications.

Keywords: Perovskite, Single crystal, Thin film, Quantum dots (QDs), Defect passivation, Solar cell, Light emitting-Diodes (LED).

1. STRUCTURE AND PROPERTIES OF PEROVSKITE MATERIALS

In 1836, Professor Rose, a German mineralogist first discovered Perovskite-type crystals in the Ural Mountains of Russia. To commemorate the Russian mineralogist Lev Perovski, this type of crystal, which can be represented by the general formula ABX_3, was named Perovskite. The feature of perovskite is that ions with very different radii can coexist stably in the same unit cell. Since the types and quantities of elements that can be accommodated in the A, B, and X positions are very wide, there exists a great amount of types of perovskite compounds. On the other hand, not all of the ion sizes get entirely adapted to the demand of high symmetry of the ideal perovskite, which commonly causes structural distortion. so the perovskite family also embraces a variety of structural distortion types.

1.1. Crystal Structure of Perovskite Materials

The general formula of an ideal perovskite is ABX_3, where A (A=Na^+, K^+, Ca^{2+}, Sr^{2+}, Pb^{2+}, Ba^{2+}, Ren^+, etc.) is a large radius cation, and B (B=Ti^{4+},Nb^{5+},Mn^{4+},Fe^{3+},Ta^{5+},Th^{4+}, Zr^{4+}, etc.) is a small radius cation and usually the transitional metals, X is an anion (X=O^{2-}, F^-, Cl^-, Br^-, I^-, etc.). In typical photoelectrical use, the organic-inorganic composite perovskite material structure is ABX_3 (A = $CH_3NH_3^+$, $HC(NH_2)^{2+}$; B = Pb^{2+}, Sn^{2+}; X = Cl^-, Br^-, I^-), in which the organic, monovalent ammonium ions partially or entirely occupy the A site instead of conventional inorganic Cs^+. The crystal structure is shown in Figure **1**, A cation is located at the 8 vertices of the cubic octahedron, the metal atom B is located at the center of the cube, and the halogen X atom is located at the center of the cube. The B atom and the X atom form a [BX_6] octahedral structure, which consists of the main framework for perovskite by co-vertex connections.

Under the influence of changes in external temperature, pressure conditions or isomorphism, the ideal ABX_3 perovskite structure (Pm3m) will undergo a series of distortions to produce phase transitions in the crystal structure, that is, from the ideal equaled crystal system to low-symmetric structure through various pathways. The ideal equaled crystal system is transformed into a tetragonal, co-square crystal system and other low-symmetric structures.

The stable perovskite structure can be judged by the tolerance factor t and the octahedral factor (R_B/R_X ratio) Calculated by formula (1), where R_A and R_B are ion radius of the cation A^+ and B^{2+} in the regular octahedral structure. R_X is the effective radius of the anion. As shown in Table **1**, to form a stable ideal perovskite structure, t should be between 0.9 and 1.0. When t<0.7, the perovskite has an ilmenite structure. When 0.7<t<0.9, the perovskite crystal has an orthogonal or tetragonal structure. When t > 1.0, the perovskite crystal presents a two-dimensional layered structure. Organic ions A^+, metal ions B^{2+} and halogen ions X^- all have obvious effects on the properties of

*Address correspondence to this author at the School of Power Engineering, Chongqing Electric Power College, Chongqing 400053, China;
E-mail: xiangjunyan@tju.edu.cn; lidewang@tju.edu.cn

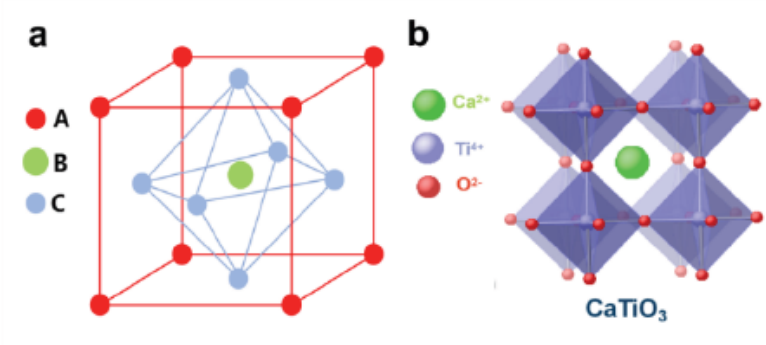

Figure 1: The crystal structure of perovskite.

perovskite materials.

$$t = \frac{R_A + R_X}{\sqrt{2}(R_B + R_X)} \quad (1)$$

Table 1: Relationship between Tolerance Factor and Crystal Structure of Organic-Inorganic Hybridperovskite

Content	Tolerance Factor (t)	Crystal Structure
1	< 0.7	Ilmenite structure
2	0.7-0.9	Orthogonal or tetragonal structure
3	0.9-1.0	Cubic structure
4	> 1.0	Layered structure

The structure diagram of perovskite is shown in Figure **2** [1]. When 0.9 <t <1, A-site ions are filled in the octahedral gap, and the perovskite crystal has a cubic structure [2]. When t<0.9, the A-site ion radius is too small to completely fill the octahedral gap, and the octahedral skeleton will be deformed. At this time, the crystal has an orthogonal structure (γ phase) or a tetragonal structure (β phase). When t> 1, the radius of the A ion is relatively large, the octahedral gap is relatively small and cannot accommodate A-site ions, the octahedrons are no longer connected at the same vertex, and the crystal presents a two-dimensional layered structure. The increase of t value will cause the change of crystal size, resulting in low-dimensional perovskite materials [3, 4].

Perovskite materials take the advantages of both organic and inorganic molecules [5]. The inorganic component provides the molecular network required for efficient carrier transport and improves the stability of the material; While the organic component makes the material have better solubility and is easy to form a film on a large area, and the preparation cost is an obvious advantage. This organic-inorganic composite perovskite material has excellent photoelectric properties such as adjustable band gap, high charge carrier mobility, strong light absorption capacity, and

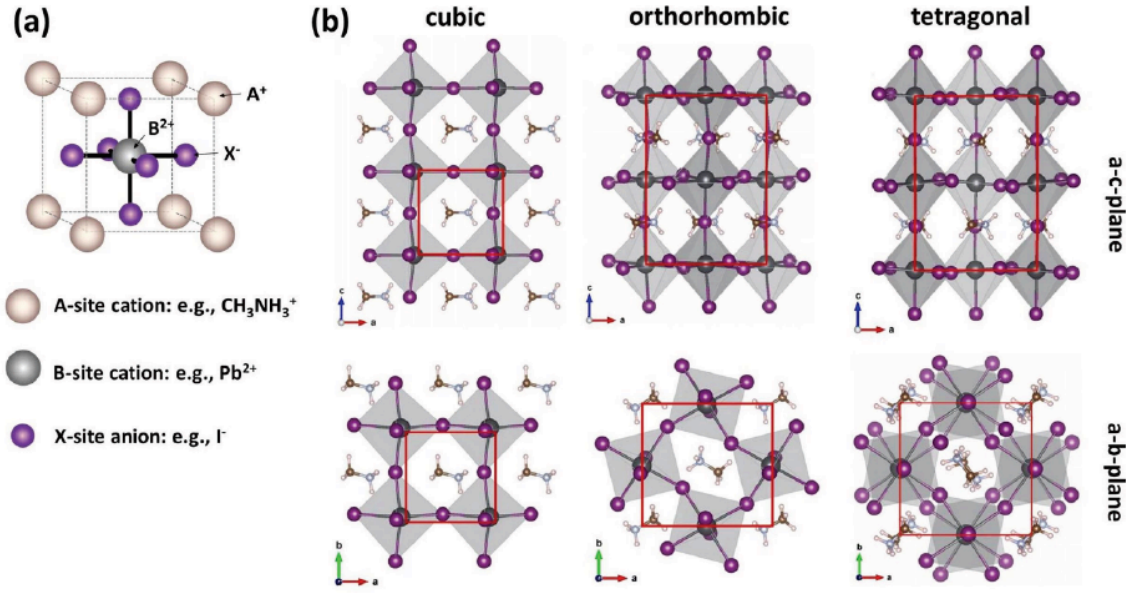

Figure 2: (**a**) Schematic of the ABX_3 perovskite crystal structure; (**b**) Comparison of cubic, orthorhombic and tetragonal perovskite phases for the prototype $CH_3NH_3PbI_3$ perovskite (top row: a-c-plane, bottom row: a-b-plane), reprinted with permission from Ref [1].

long electron-hole carrier diffusion length [6-9]. Therefore, it is widely used in solar cells [10-12], light-emitting diodes (LED) [13, 14], photodetectors [15-17] and other fields [18-21]. These fields require relatively high quality of perovskite crystals or films.

1.2. Two-Dimensional Perovskite Material Structure and Characteristics

When a larger cation is introduced into the three-dimensional perovskite, the original cubic structure of the material is destroyed, and the interconnected [BX_6] octahedrons separate in a certain direction and become a two-dimensional perovskite with a layered structure. Compared with three-dimensional materials, two-dimensional perovskites have many excellent physical properties due to their unique surface effects, small size effects and quantum effects. It has better environmental stability and can precisely control the thickness of the n-layer through simple chemical methods to adjust the electronic structure of the material. Two-dimensional perovskite materials are also easy to chemically modify and it is easy to adjust its properties through doping. Two-dimensional materials present higher atom utilization, lower defect density, better environmental stability [22], higher carrier mobility [23], and longer carrier lifetime [24].

The [BX_6] octahedron in the two-dimensional perovskite has three connection methods: corner-sharing, edge-sharing, and face-sharing, as can be seen in Figure **3a** [25]. Among them, the corner connection is the main octahedral composition. Generally speaking, two-dimensional perovskites satisfy the Ruddlesden-Popper (RP-) phase formula, namely $A_2A'_{n-1}B_n X_{3n+1}$ [26], where RNH_3 is the large organic ammonium cation with long aliphatic chains or aromatic groups, and n is the number of octahedral stacked layers between the two cations. When n = 1, it means there is only a layer of inorganic octahedron, and the perovskite has a two-dimensional structure; when n = ∞, the perovskite has a three-dimensional structure; when n is a certain low value (2~5), it is defined as quasi-two-dimensional structure (Figure **3b**).

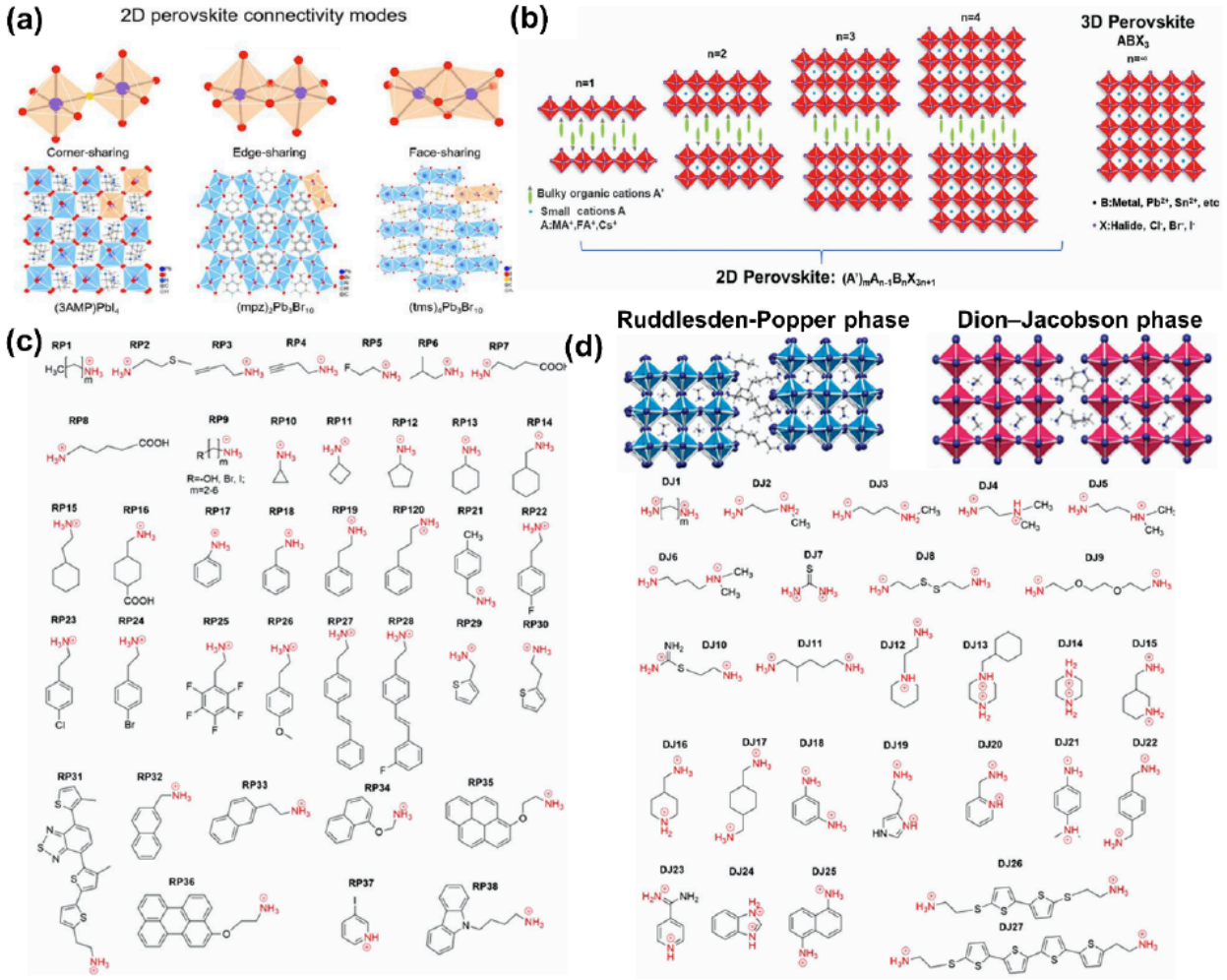

Figure 3: (**a**) Connectivity modes in 2D perovskitecorner-sharing, edge-sharing, face-sharing [25]; (**b**) Schematics of 2D perovskites(n=1), quasi-2D perovskites (n=2~5) and normal 3D perovskite (infinitive n); Summary of different bulky cations for RP-(**c**) and (**d**) DJ-phase 2D perovskites [29].

From three-dimension to two-dimension, the tolerance factor t can be adjusted simply by changing the size of the organic spacer cation, so that t>1 makes the 2D-perovskite structure stable. The two-dimensional perovskites have improved chemical stability due to the hydrophobicity of the organic spacer group in the two-dimensional perovskite [27]. For example, n-butylamine (BA) and phenethylamine (PEA) organic cations are commonly used in two-dimensional perovskites. Moreover, Yuan *et al.* explored the synergy of BA^+ and F-PEA^+ along with adjusting A sites of MA^+/FA^+ ions [28]. The introduction of F-PEA^+ induces an ordered distribution of the film from low-n to high-n phases, resulting in enhanced crystallinity and grain size, fewer cracks or voids as well as preferred orientation. Under the cooperation effect, the obvious elevation in the efficiency of NiOx-based $(BA_{0.9}F\text{-}PEA_{0.1})_2(MA_{0.8}FA_{0.2})_3Pb_4I_{13}$ n = 4 quasi-2D RP perovskite solar cells from 12.51 to 15.68% was achieved. Other ever-reported organic spacers for RP- two-dimensional perovskite construction has been summarized in Figure **3c** [29]. Similarly, symmetric diamine compounds with two amino groups can avoid any gaps by forming hydrogen bonds on both ends with the two adjacent inorganic sheets, leading to a more stable (DJ-) phase 2D perovskite with $A'A_{n-1}B_nX_{3n+1}$ stoichiometry, as shown in Figure **3d**, along with their applicable molecular structures.

In some special cases, the term “two-dimensional” only refers to the shape control into a nano/microscale morphology, usually the well know nanosheets or nanoplates, while doesn’t necessarily mean the two-dimensional nature of unit cells. Such size reduction is usually correlated with the quantum size effect, or catering the carrier diffusion length limit to suppress bulk recombination. Yehonadav Bekenstei et al. synthesized two-dimensional inorganic perovskite $CsPbBr_3$ with different thicknesses, and the luminescence peak position of the two-dimensional inorganic perovskite $CsPbBr_3$ was red-shifted as the thickness of the nanosheet increases [29]. Wu reported that the quantum yield of $CsPbBr_3$ nanosheets was as high as 96% [30]. This was because the defect state density of perovskite materials decreased as the dimension decreased, and the low defect density improved the radiation recombination efficiency, which made two-dimensional perovskite material highly fluorescence efficient.

More recently, two-dimensional perovskite materials with the combination of other two-dimensional materials (both in crystallography and in morphology, such as transition metal disulfides, grapheme [31-33], etc., using as wearable smart devices and flexible energy storage devices have emerged as a tendency to obtain optoelectronic devices with excellent performance. Therefore, exploring the optical and electrical properties of two-dimensional perovskite materials promises vital significance both in scientific research and innovative device development.

2. PREPARATION OF PEROVSKITE MATERIALS

The unique optoelectronic properties in particular, high electron/hole mobility, long carrier diffusion length, and wide spectral absorption range were widely underlined by the researchers. However, such advantages of perovskites rely heavily on the quality of crystal architecture. The crystallization process of perovskite crystals is closely related to the morphology of the film, trap states, which in turn affects the photoelectric properties such as the charge separation and extraction efficiency of the device, the recombination process, and the charge carrier mobility. Therefore, the preparation of high-quality perovskite crystals and films has become an important prerequisite for the application of perovskites.

Crystal synthesis mechanisms of perovskite materials include solution cooling crystallization method, inverse crystallization method, and auxiliary crystallization method. The perovskite film fabrication methods include spin coating, blade coating, printing, and vapor deposition. The preparation process and principles and control conditions are explained in the following categories.

2.1. Preparation of Perovskite Crystals

The conventional 3D perovskite crystals are regularly and periodically arranged in a three-dimensional space. Compared with the perovskite film, the perovskite single crystal has better uniformity, and has a wider light absorption range than the corresponding polycrystalline film [34-36]. This is very important for studying the photoelectric properties of perovskite such as carrier diffusion, recombination and lifetime.

Single crystal processing and preparation are simple and low cost. Because of its adjustable color, narrow emission band, simple synthesis, convenient processing, it has been widely used in fields including light-emitting devices and photodetectors.

2.1.1. Solution Cooling Crystallization Method

The self-nucleation of single crystals mainly depends on that the solubility in the solvent decreases with the decreasing temperature, and the single crystal materials are obtained by slowly lowering the temperature of the solution. Tao [37] *et al*. adopted the bottom seeded solution growth method to first obtain

small seeds by lowering the temperature of the solution, then adds them to the solution to provide heterogeneous nucleation sites and induce crystallization to obtain large size $CH_3NH_3PbCl_3$ single crystal. The size of the $CH_3NH_3PbI_3$ single crystal reached 71 mm×54 mm×39 mm. In the process of cultivating single crystals, they found that the crystal growth rate is proportional to the total surface area of the crystal seed. By analyzing the evolution process of the crystal seed shape, they proposed a seed-induced heterogeneous nucleation mechanism to deduce the crystal growth process.

Ma's team [38] treated the surface of the substrate with a limited gap to provide favorable conditions for the preparation of large-area single crystal perovskite films. Specifically, the silicon surface is hydrophobically treated to increase the nucleation barrier, and the ITO surface is plasma cleaned to reduce the nucleation barrier and activate the dangling bonds on the ITO surface, so that the perovskite will interact with the ITO during the crystal growth process. The surface forms a stronger bond. The silicon substrate and the ITO substrate are sandwiched together to form a certain gap, then the perovskite precursor solution was dropped on the edge of the ITO bottom, followed by absorbed into the gap under capillary force. The substrate was placed on a hotplate at 80°C and applied with a certain pressure. The growth of the single crystal perovskite film was completed after 24 h. A single crystal film of $MAPbBr_3$ with the thickness of hundred nanometers could be obtained by adjusting the applied pressure.

The wettability of the substrate also affects the formation of perovskite single crystals. The thickness of the perovskite layer in the overall device limits the grain size of the halide perovskite film. For substrates with poor wettability, the droplets of the precursor solution will disperse. The material growth base on theses droplets. Since the distance between the droplets is longer, the crystal grains produced are larger. The crystal grains with high average aspect ratio of 2.3- 7.9 and no pinholes were synthesized effectively owing to the heterogeneous nucleation suppression. The fewer the grain boundaries, the better the crystallinity are necessary for thin film with large grains [39]. Finally, device achieved 18.3% efficiency with high stability.

2.1.2. Inverse Temperature Crystallization Method

The inverse crystallization method is based on the abnormal phenomenon that the solubility in a specific solvent decreases with increasing temperature. The specific solvents are N,N-Dimethylformamide(DMF), Dimethyl sulfoxide(DMSO) and Gamma-butyrolactone (GBL). In this way, the retrograde solubility of halide perovskites helps to synthesize millimeter-sized crystals. For example, to prepare $FAPbI_3$ single crystal by adjusting the temperature of the precursors in GBL, the temperature is elevated from 80 to 120°C. Similarly, a single crystal of $FAPbBr_3$ can be grown by increasing the temperature of the precursor solution made of $PbBr_2$ and FABr in a mixture of DMF and GBL (1:1 v/v). Here, by reducing the solubility of the precursor, GBL helps crystal growth. Also, inorganic perovskite single crystals can be prepared by inversion crystallization. Drin *et al.* used this method to prepare $CsPbBr_3$ single crystals. The molar ratio of cesium lead bromide (CsBr) and lead bromide ($PbBr_2$) was 0.5:1. They were dissolved in DMSO and heated to 70°C, and then cyclohexanol and DMF were added. The crystals were first heated to 90°C to form crystal nucleation, and then heated to 110°C to further grow crystals [40]. Ethyl acetate and dichloromethane are sometimes used as anti-solvents to accelerate the saturation as the alternative of temperature elevation [25].

2.1.3. Assisted Crystallization Method

Single crystals can be derived either spontaneously, or with the aid of external conditional changes and add additives, to assist single crystals to grow faster while still retaining the high quality. Bakr's team [41] developed a new growth method based on a cavitation-assisted asymmetrical crystallization strategy, which would promote heterogeneous nucleation by providing enough energy to overcome the nucleation barrier. They successfully prepared a single crystal film of $MAPbBr_3$ with a thickness of 1-60 μm under the assistance of ultrasound. They proposed the surface tension plays a central role in the nucleation and growth of crystals [42]. In addition, Liu's team [43] developed a local temperature reduction induced crystallization method to directly obtain lead-free perovskite wafer $MASnI_3$ with a thickness of about 110 μm and a lateral size of 1 cm in an oil bath.

Additive engineering in precursors or the anti-solvents are most commonly reported to facilitate better crystal growth, which could be identified as additive-assisted crystallization. Wang *et al*. added moderate amount of imidazolium (IA) to $MAPbI_3$. Due to its strong Lewis base to coordinate with adjacent electron-deficient ions in the lattice, the mixed cationic halide perovskite has fewer defects and better morphology [44]. Gupta reported that the anti-solvent accelerated reverse temperature crystallization method was also used to synthesize high-quality, large- crystal perovskite with a size of 1 cm at room temperature [45]. They revealed the role of various growth parameters such as temperatures and precursor compositions (amount of anti-solvent and solution polarity) during crystal growth in attaining the suitable condition for

crystal. It was found that even at very high temperatures (140°C), precise control of the anti-solvent (Acetonitrile) and solution molarity helps to achieve better crystal growth.

Anti-solvent vapor assisted crystallization adopts vaporized anti-solvent to interact with the precursor solution, resulting in the co-precipitation into high-quality crystals. Large interaction areas can be ensured by controlling the diffusion of vapor. Tidhar *et al*. first used this method to synthesize $MAPbBr_3$ [46]. The growth of $MAPbI_3$ single crystal failed in the case of alcohol as an anti-solvent. Shi *et al*. used DCM instead of ethanol and produced crack-free single crystals of $MAPbI_3$ with a size of more than 100 mm^3 [47]. They also reported that high-quality $CH_3NH_3PbI_3$ and $CH_3NH_3PbBr_3$ single crystals were obtained by vapor-assisted deposition. The vials containing the precursor solutions of $CH_3NH_3PbI_3$ and $CH_3NH_3PbBr_3$ was put into a beaker containing DCM. DCM slowly diffuses into the precursor solution to form crystal nuclei and further grow into crystals. The obtained single crystal has low density of defect states (10^9-10^{10} cm^3) [47].

Acyl halide is usually used as a multi-purpose component in organic chemical reactions. It is famous for its strong reaction to nucleophilic compounds, and can form carboxylic acid derivatives. It is possible to synthesize all inorganic or organic-inorganic $APbX_3$ and control the optical properties [48] by adjusting the relative amount of cationic precursor, ligand, solvent. The $MAPbX_3$ perovskite synthesized in this way have a cubic morphology and high phase purity. The synthesized perovskite has a narrow emission line width of 15 ~ 43 nm, and the PLQY of $MAPbBr_3$ is as high as 92%.

2.1.4. Hot Injection Method

Apart from the single-crystals or large-grains in polycrystals, perovskite colloidal, as small as quantum dots, is another widely adopted morphology, sometimes for perovskite solar cells [49], while mostly suitable for perovskite light-emitting diodes (PeLEDs) as schemed in Figure **4a** [50]. Such materials provide compatibility with preparing inks for patterned printing. The precise control towards the nanoparticle size (in most cases less than 10 nm) effectively tailor the energy level structures that bandgap gradually turned expanded (Figure **4b**). This phenomenon is called The Quantum Confinement Effect. The mechanism could be interpreted as that the excitons, consisting of a pair of an electron and a hole, are bound by Coulomb attraction inside the semiconducting materials. There is a critical threshold parameter of Bohr radius (R_B) radius representing the electron−hole pair orbit, which is determined according to the equation (2),

$$R_B = \frac{\varepsilon_0 h^2}{e^2}\left(\frac{1}{m_e^*}+\frac{1}{m_h^*}\right) \quad (2)$$

where R_B is a Bohr radius, $\hbar$ is the reduced Planck constant, ε_0 is the permittivity of the vacuum, *e* is the elementary charge, and m_e*and m_h* are the effective mass of the electron and hole, respectively. The Quantum Confinement Effect occurs when the particle size is smaller than its R_B, in which case the particle could be defined as quantum dots (QDs). The enlarged bandgap could be further quantitatively descripted by equation (3),

$$E_{g(QDs)} = E_{g(bulk)}+\frac{h^2}{8R^2}\left(\frac{1}{m_e^*}+\frac{1}{m_h^*}\right)-\frac{1.786e^2}{4\pi\varepsilon_0\varepsilon_r R^2} \quad (3)$$

where $E_{g(bulk)}$ is the bandgap of the bulk material, and ε_r is relative permittivity. This approach provides another alternative to adjust bandgap and color other than doping/alloying strategy on A-site or X-site, avoiding the detrimental phase segregation among the mixed ions during operation or even aging.

Such small QDs possess high specific surface areas with strong aggregation tendency, therefore must be stabilized and separated by amphiphilic ligands whether during or after QD crystal synthesis. The surfactant ligands self-assembled into micelles in the oil phase, and allowed the precursor ions gradually diffused into itself with the aid of elevated temperature. This synthesis method, *i.e*., the hot injection, presents the big generality for most kinds of quantum dots, no exceptions of the perovskite species (Figure **4c**). The crystallization confined in respective micelles could be divided into two basic process of nucleation and growth. The nucleation involves the formation of small clusters that act as seeds for growth. The rate of nucleation and the size of the nucleus depend on the concentration of the precursor, the solvent, and the reaction temperature [51]. The formed nuclei begin to grow by the addition of precursor molecules. The growth process can occur by ion-by-ion growth process, which is highly dependent on the precursor concentration, reaction temperature, and reaction time. At low concentrations and moderate temperatures, the growth is slow and could be easily controlled. After reaction, the ligand remains absorbed on the QD surface. Generally, a polarized functional group strongly interact with the unsaturated surface ions of the QDs, so oriented towards the QD, while the long aliphatic chains point towards the solvent.

It should be addressed that the insufficient bonding or micelle concentration results in moderate adsorption-desorption balance, so the momentary protection lost in this dynamic process usually results in secondary growth of irregular coalescence or fusion of the QDs. Further ligand exchanging is a prevailing

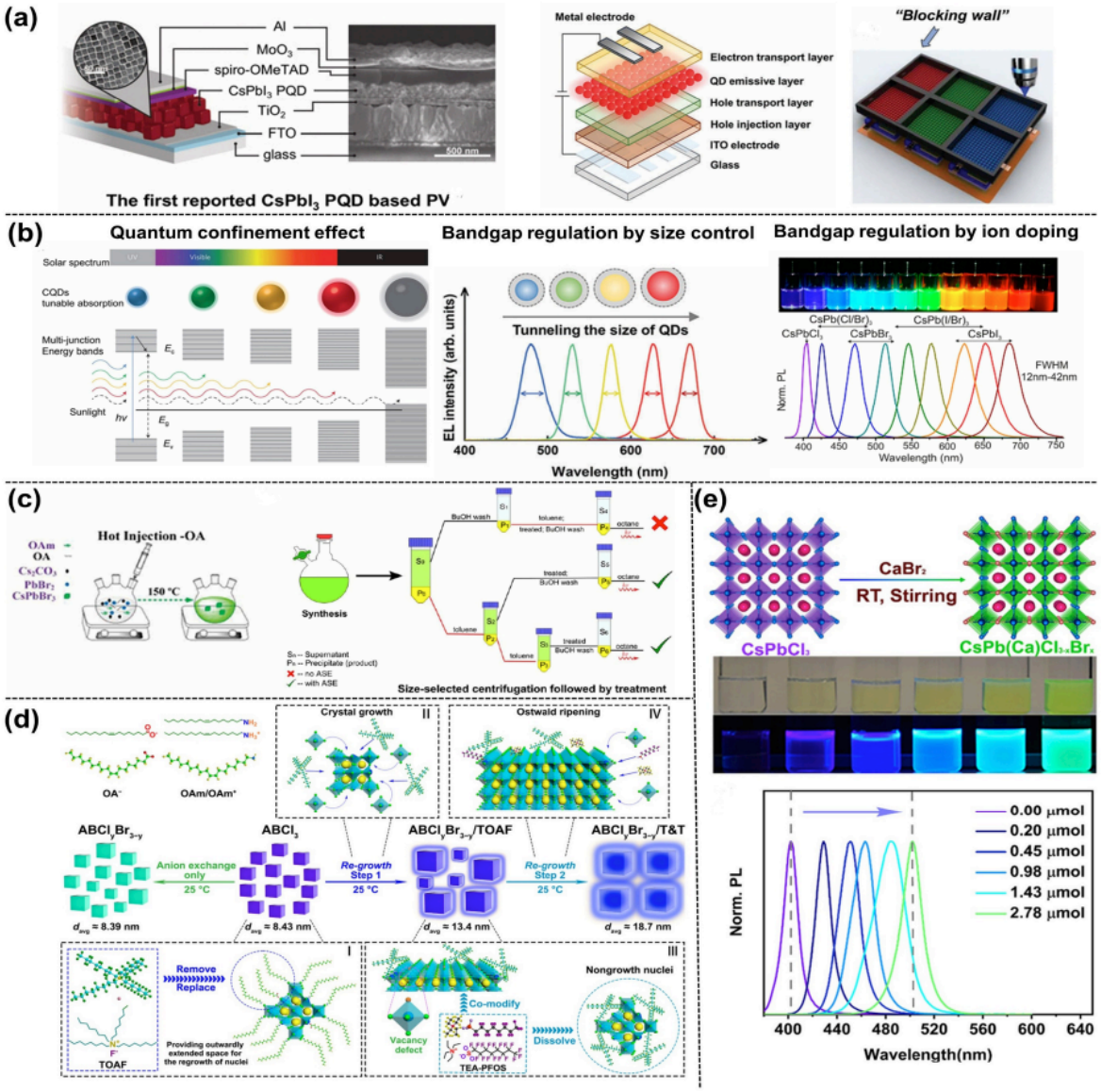

Figure 4: (**a**) Device structures of QD-based photovoltaics (left)[49], light-emitting diodes (middle) and its printing process (right) for RGB (red/green/blue) colorful display [50]. (**b**) Bandgap tenability based on quantum size effect or ion doping [50, 51]. (**c**) Schematic of hot injection for quantum dot synthesis and following purification by centrifution [51]. (**d**) Co-regulation strategy dominated by double short molecules permitting the regrowth of quantum dots for efficient deep-blue emitting [52]. (**e**) Ca^{2+} induced highly fluorescent $CsPb(Br/Cl)_3$ perovskite quantum dots via fast Anion-Exchange and Cation-Doping [53].

optimization strategy to overcome this challenge. The conventional oleic acid (OA) and Oleylamine (OAm) system could be exchanged by other ligands with higher polarity for inducing higher binding energy, as well as the orientation rearrangement. For instance, our group demonstrated a two-step ligand treatment of subsequent TOAF and TEA-POFS (Figure **4d**) [52]. The first exchanging by the TOAF ligand with high steric hindrance of the branched chain significantly loosened the surface adsorption to realize controlled secondary growth via Ostwald ripening, followed by re-anchoring by the strongest interaction from TEA^+ and dense adsorption because of its short chain. Despite of the small crystal sizes, the crystallinity could also be improved to some extent as the result of less surface defect densities. A marked increase of photoluminescent quantum yield (PLQY) was obtained from 58.67% to 99.26% for blue emission. Another effective strategy aims at the intrinsic lattice (bulk) stabilization by element doping. After $CaBr_2$ were doped into the $CsPbCl_3$ precursors, the stable $CsPb(Ca)Cl_{3-x}Br_x$ QDs were obtained, in which Br^- were applied for red-shift to targeted blue emission, while the Ca^{2+} greatly induce the rapid ion exchange during hot injection and supplement the Pb^{2+} vacancy (Figure **4e**) [53]. The ideal PLQY over 99.9% at 470 nm blue emission verified its potential for further QLED device application.

2.2. Thin Film Preparation of Perovskite

High-quality perovskite devices require that the perovskite must have good crystallinity, large grain size,

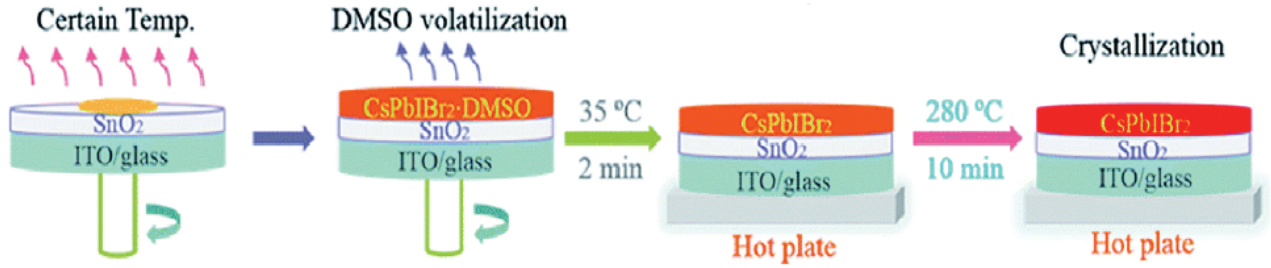

Figure 5: Illustration of $CsPbIBr_2$ perovskite film fabrication. Reprinted with permission from Ref. [61].

and few grain boundaries compatible with the film fabrication process. This chapter mainly introduces spin coating method, blade coating method, vapor deposition method, and printing method.

2.2.1. Spin Coating Method

The quality of the perovskite film plays a key role in the photovoltaic performance of the perovskite. For the preparation of high-efficiency solar cells, a dense and well-crystallized perovskite film free of pinholes, thickness fluctuations and cracks is the basic prerequisite about the surface coverage [54]. The uniform film can be obtained by a very simple, cost effective and rapid spin coating solution.

The film crystallization could similarly be divided into successive solution supersaturation, nucleation, and growth into large crystals in detail [55-58]. Though the convective diffusion is conducive to the slow evaporation of the solvent, simple spin coating cannot produce a perovskite layer of uniform thickness in a wide range [59]. Li's team [60] obtained a bright and smooth $FA_{0.81}MA_{0.15}PbI_{2.51}Br_{0.45}$ crystalline film by introducing a simple vacuum flash one-step spin coating method. Yin's [61] team obtained $CsPbIBr_2$ films with preheating process. The process of preparing $CsPbIBr_2$ perovskite film by preheating assisted spin coating method is shown in Figure **5**. The SnO_2/ITO substrate on the hot plate bake for 10 min, and $PbBr_2$ and CsI were dissolved in DMSO at room temperature to prepare the $CsPbIBr_2$ precursor. The precursor solution was spin-coated on the preheated SnO_2/ITO substrate at a temperature of 35°C, 5000 r/min for 60 s, then a two- step annealing process was performed to obtain the perovskite film. This is an effective method for preparing high-quality inorganic perovskites.

However, bromine-rich perovskites such as $CsPbBr_3$ have been troubled by traditional two-step deposition methods [60, 62]. Liao's team [63] reported a simple and improved multi-step spin coating process for manufacturing high-quality $CsPbBr_3$ films, as shown in Figure **6**. The film prepared has higher uniformity, higher $CsPbBr_3$ phase purity and larger average grain size. More importantly, not only PCE of the $CsPbBr_3$ perovskite cell was significantly improved, but also the humidity and thermal stability of the unsealed $CsPbBr_3$ perovskite solar cell in the environment were improved.

2.2.2. Blade Coating Method

Perovskite solar cells are recognized as having great potential for industrialization. However, the current perovskite solar cells are faced with many challenges from the spin- coating method: large loss of materials and low of production efficiency, which is not suitable for scalable production.

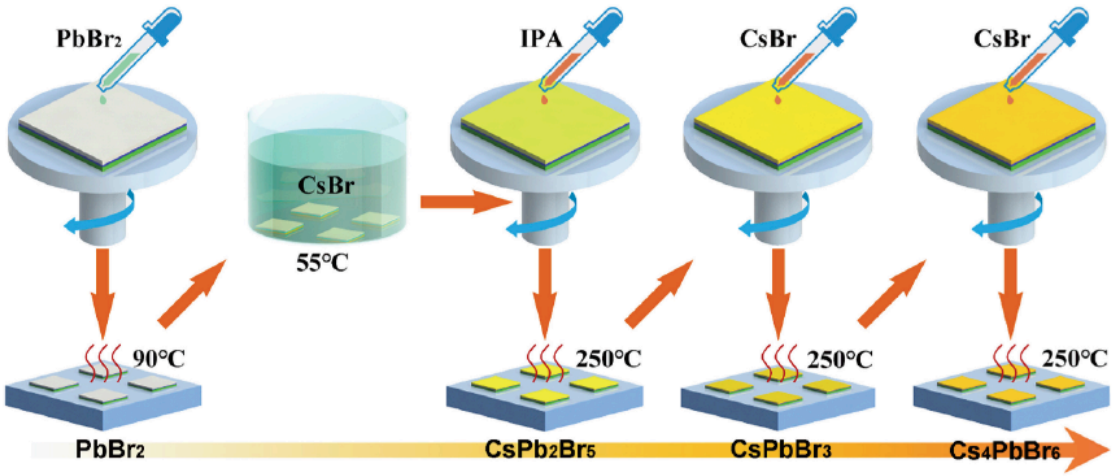

Figure 6: Multi-step spin-coating method. Reprinted with permission from Ref. [63].

Processing in glove box limits the large-scale production of perovskite cells, and the use of glass substrate limits its range of applications. The blade coating one-step method is used in the perovskite layer preparation, which is simple and effective. The quality of the film can be controlled. Scratch coating technology is a simple, environmentally friendly, low-cost method for manufacturing optoelectronic devices [64, 65]. This technology can produce a uniform film over a large area while avoiding waste of material [66]. The morphology of the perovskite film coated on the blade can be controlled by adjusting the height of the blade, the speed of the blade, the volume and viscosity of the precursor solution [64, 67].

Humidity plays an important role in determining the perovskite layer morphological quality and the performance of related equipment. Yang *et al*. [64] controlled the RH to evaluate its impact on the blade coating perovskite [68]. The overall light absorption, crystallinity and the perovskite film surface coverage increase significantly as the environmental humidity decreases during the doctor blade coating process (Figure **7a**). However, it can be inferred that the film formation process is slightly similar to the spin coating process [69, 70] because the resulting films show similar morphological trends (Figure **7b**) [64].

It is believed that the blade coating technology can replace the traditional spin coating technology to produce industrial perovskite in the future. Kim *et al*. [71] reported that the difference in PCE of PSC prepared with a doctor blade coating in ambient air was only 0.78% compared to a device prepared in a glove box containing N_2. Wang *et al*. [72] reported that the PSC with a device structure of ITO / NiOx / 4-bromobenzoic acid / perovskite / PCBM / bis-C_{60} / Ag has a PCE of 11.1% at a humidity of 40-50%. All layers are prepared by doctor blade coating, indicating the coating technology has shown great potential for expanding the scale of perovskite cells. Deng *et al*. [73] further confirmed the utility of the blade coating method for the production of commercial-scale solar modules. They successfully used a doctor blade to create a solar device with an effective area of more than 50 cm^2 and an efficiency of about 15%.

Liu's team tracked the phase transition and crystal growth process of perovskite under different film forming conditions, as shown in Figure **8** [74]. In the process of squeegee-blade coating, it was found that the method of inducing rapid solvent removal by thermal substrate can effectively inhibit the appearance of perovskite intermediates, thereby preparing large-grain perovskite film with high crystalline quality. At the same time, it also revealed that the phase transition process of the perovskite film from the disordered precursor sol-gel phase to the perovskite phase has an important impact on the film quality, photophysical properties and photovoltaic performance of the device. Regulating this transition process, the high-quality $MAPbI_3$ film prepared by blade coating in air finally achieved 18.74% photoelectric conversion efficiency in a 0.09 cm^2 small area device and a 1 cm^2 large area device. The efficiency of 17.06% used to be the highest level in the world in the same field. The research results provided important theoretical support for the transfer of perovskite preparation to printing method, and will help further promote the large-scale commercial application of perovskite solar cells.

2.2.3. Printing Method

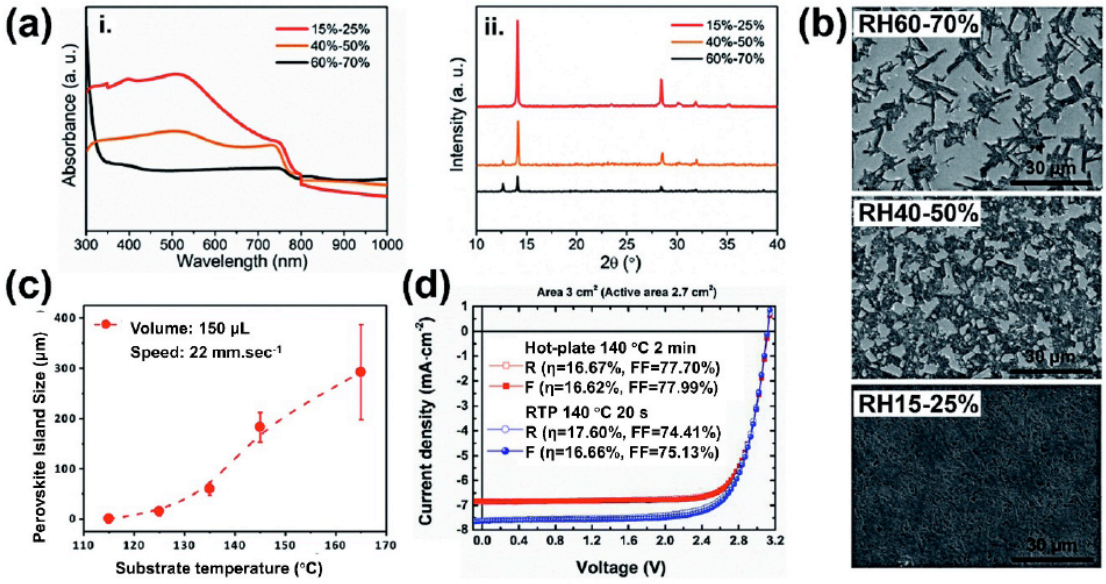

Figure 7: (**a**) UV-vis absorption spectra and X-ray diffraction curves of the perovskite layer blade-coated at various RH levels. (**b**) SEM images of perovskite blade-coated at different RH levels. (**c**) Size of perovskite islands related to substrate temperature during blade-coating. (**d**) J–V curves of perovskite mini-modules prepared in air using RTP and hot-plate annealing. Ref. [68].

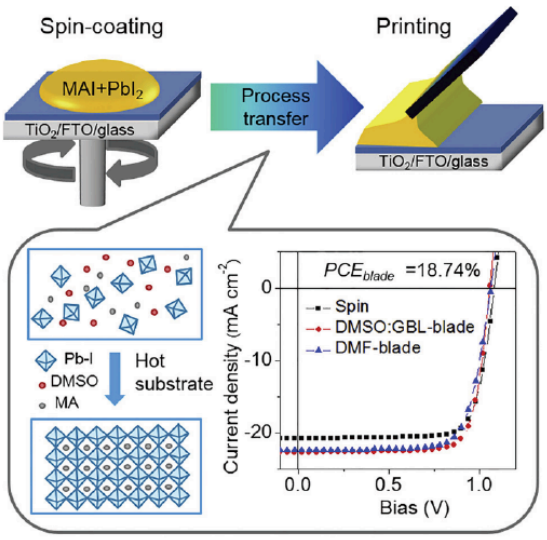

Figure 8: blade coating process Ref [74].

Inkjet printing is an easy technique that can selectively realize the deposition mode of functional materials [82, 83]. To prepare perovskite films by inkjet printing, the size and thickness of the film can be adjusted by the size and number of the prepared seed crystals. The basic procedure of this method is to first form a patterned perovskite seed on the substrate, and then cover it on the target substrate with a saturated perovskite solution. The single crystal film in-situ grows on the seed when the solvent evaporates. The key to prepare the perovskite seeds on the substrate is to introduce the perovskite seed molds into the liquid membrane system. Seeds play a decisive role in the formation of single crystal films because they can regulate the order and uniform growth and more importantly, let shaping the single crystal into films come true.

To suppress the random nucleation problem in the crystallization process, Gu [84] and others innovatively introduced the seed template prepared by printing into the crystallization system, and proposed a controllable printing method for preparing perovskite using seed template. (Figure **9**) The researchers first prepared

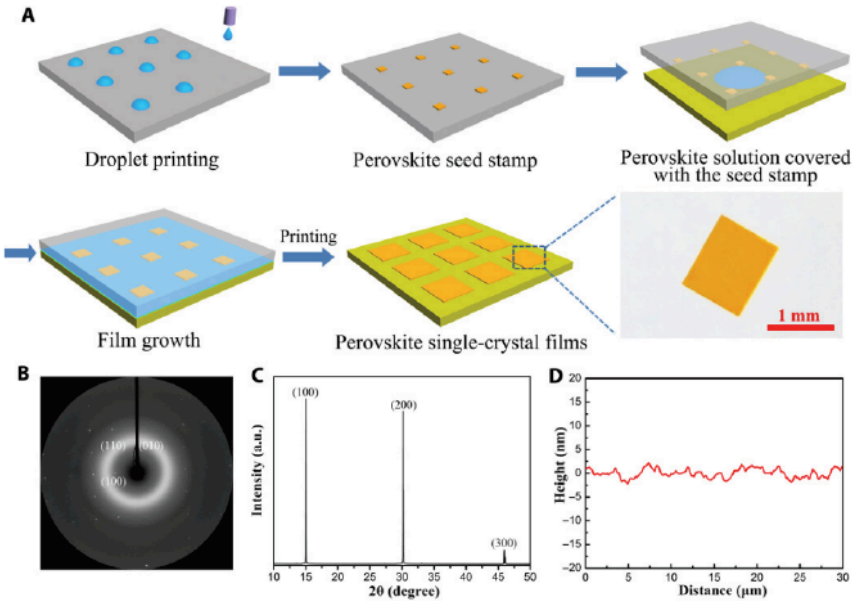

Figure 9: Seed printing of perovskite single-crystal films. (**A**) Schematic illustration of the scalable growth of perovskite single-crystal films. First, perovskite seed stamp is fabricated using an inkjet printing method. Second, the prepared seed stamp is covered on the target substrate with perovskite solution, and perovskite single-crystal films in situ grow as the solvent dries. Taking away the covered stamp, we printed the perovskite single-crystal films on the substrate. Scale bar, 1 mm. (**B**) Synchrotron radiated single-crystal XRD photograph of the perovskite film on quartz glass by rotating the incident x-ray angle of ±22.5°. All the diffraction rings belonged to the quartz glass substrate. (**C**) XRD pattern for the perovskite single-crystal film a.u. arbitrary units. (**D**) AFM profile of the perovskite single-crystal film surface. Ref. [84].

perovskite seed crystals on a hydrophobic substrate by inkjet printing, and then covered the seeded template with a saturated solution of perovskite. Studies have found that introducing a seed template into the crystallization system can effectively change the precursor ion distribution in the system and reduce the random nucleation density during the crystallization process, thereby achieving a controllable preparation of perovskite single crystal films. The imprinting of the perovskite seed can make perovskite single crystal film adaptable on the most conventional substrate such as molybdenum disulfide (MoS_2) and graphene. Crystal growth can be precisely controlled by imprinting of the perovskite seed.

By adjusting the size of the seed crystal prepared by printing, the thickness of the perovskite single crystal film can be effectively adjusted. The perovskite single crystal film prepared by printing has high crystalline quality and can be directly used for photoelectric devices such as photodetectors and image sensors. The detector prepared by this method has an ultra-low dark current of 1.7 nA and a responsivity up to 40 A/W. This printable strategy also allows controlled growth of perovskite single crystal films on various substrates to achieve high yields.

2.2.4. Vapor Deposition Method

The vapor deposition method is always carried out in a clean environment. This method avoids the uncontrollable influences from solvents. The film thickness can be monitored and controlled to obtain a more uniform film. Because of the lower preparation temperature, vacuum deposition is compatible with a lot of substrates, such as flexible substrates and textiles. One advantage of the dual-source vapor deposition method is that it can prepare high-crystallinity perovskite films of any thickness and monitor the growth of materials in real time [75]. Mitzi and his colleagues [76] prepared organic-inorganic hybrid perovskites by using a single source thermal ablation equipment (Figure **10a**), including $(C_6H_5C_2H_4NH_3)_2PbI_4$, $(C_6H_5C_2H_4NH_3)_2PbBr_4$ and $(C_4H_9\text{-}NH_3)_2SnI_4$. Snaith's group [77] prepared a uniform flat film of mixed halide perovskite $CH_3NH_3PbI_{3-x}Cl_x$ by dual-source vapor deposition. Figure **10b** shows a diagram of the vapor deposition device. These examples show that this technology can be used to prepare metal halide perovskite perovskites.

Liu *et al*. reported that when the furnace temperature was increased from 320°C to 330°C, lamellae were almost invisible at lower pressure. More obvious changes in the perovskite structure can be observed, which are composed of connected (Figure **10**) when the temperature is maintained at 330°C and the pressure changes. When the temperature was reached to 340°C, the evolution of the perovskite morphology was similar to that at 330°C, but the lamellae tended to connect together and form a thick stepped structure. At last, it can be found that the film can be decomposed into an amorphous structure under high growth temperature and low pressure [78].

Mi *et al*. [79] cooperated with Wu group found that during growing $MAPbBr_3$ by CVD, the growth temperature had vital influence on the morphology of $MAPbBr_3$ single crystal. Jin's team [80] used an in-tube vapor deposition device to grow $CsPbBr_3$ single crystal films, in which increasing the reaction temperature is important for achieving sustained growth of $CsPbBr_3$ single crystals. Temperature increasing enhances the adsorbed atoms diffusion, but also accelerates the first epitaxial crystal nucleation.

Zeng's team [81] obtained ultra-thin $CsPbBr_3$ film on ultra-thin mica, and also succeeded in cultivating $CsPbBr_3$ ultra-thin films on different substrates by chemical vapor deposition. It can be seen from Figure **11** at different substrates with different morphology and quality have different inhibitory effects on $CsPbBr_3$ ultra-thin films.

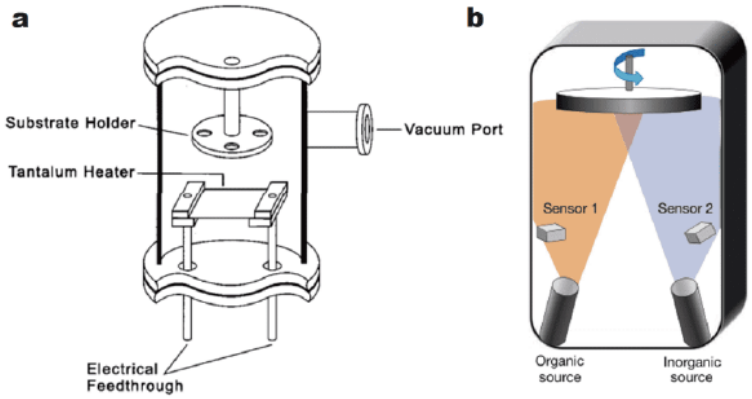

Figure 10: (**a**) Cross sectional view of single source thermal ablation chamber. Reprinted with permission from Ref [76]. (**b**) Dual-source thermal evaporation system for depositing the perovskite absorbers. Reprinted with permission from Ref. [77].

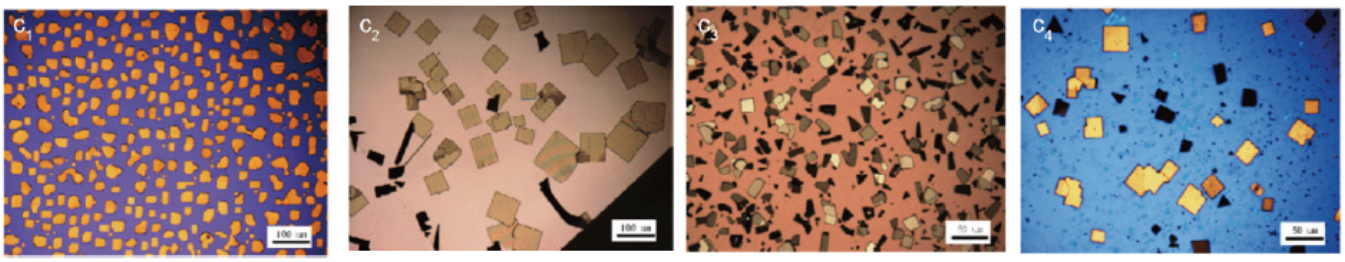

Figure 11: Optical images of $CsPbBr_3$ ultrathin platelets on different substrates (**c1**) SiO_2/Si, (**c2**) GaN, (**c3**) FTO glass, (**c4**) graphene. Reprinted with permission from Ref. [81].

3. THE PERFORMANCE AND CONTROL OF PEROVSKITE

The previous chapter introduced various conditions and methods for preparing perovskite materials, but there are inevitable defects in the preparation process. Small grains with large occupation of grain boundaries, unsaturated bonds bringing deep-level defects on surfaces, and yet dense film formation are undesirable. These shortcomings can cause problems such as non-radiative recombination and unbalanced carrier transport. Investigating and inhibiting the defects in perovskite films has become the next research hotspot.

3.1. Performance Characterization

3.1.1. Charge Carrier Dynamics

Perovskite illustrates the advantages in optical coefficient, high carrier mobility, longer carrier lifetime and diffusion length. These advantages are mainly derived from the generation of carriers and excitons. The recombination dynamics of charge carriers in perovskite is shown in Figure **12** [85]. it can be perceived that the excitons are freely diffused or bonded. The dynamic characteristics of free carriers are the diffusion coefficient ($D_{n,p}$) and carrier mobility (μn, p), which are related through Einstein's equation (4):

$$\mu_{n,p} = \frac{eD_{n,p}}{k_B T} \tag{4}$$

where e is electric charge, K_B is Boltzmann's constant, and T is temperature. The diffusion length (*L*D) of charge carriers is related to their mobility or diffusion coefficient according the equation (5): [34].

$$L_D = \left(\frac{k_B T \mu_{n,p} \tau}{e}\right)^{\frac{1}{2}} = (D_{n,p}\tau)^{1/2} \tag{5}$$

where τ is the lifetime detected from the time-resolved photo-luminescent spectroscopy (TRPL) . When thermal energy (K_B T) overcomes the exciton binding energy, the long PL lifetimes of single crystal perovskites and thin film perovskites indicate the existence of free carriers formed by the dissociation of photogenerated excitons.

3.2. Performance Control

Perovskites exhibit a variety of structural defects due to its ionic properties [86]. Figure **13** illustrates the most important types of defects on the surface or grain boundaries of polycrystalline perovskite films, including the inherent point defects that form shallow level traps, such as I^- or MA^+ vacancies. The carriers trapped here is easily excited to conduction band again because the ambient phonon energy (k_BT) is mostly enough to overcome the low exciton binding energy. On the contrary, other deep-level (closed to the middle of the bandgap) defects will produce strong non-radiative loss. Therefore, the use of additives, solvent engineering, and interface engineering are necessary provide functional groups with a series of non-covalent

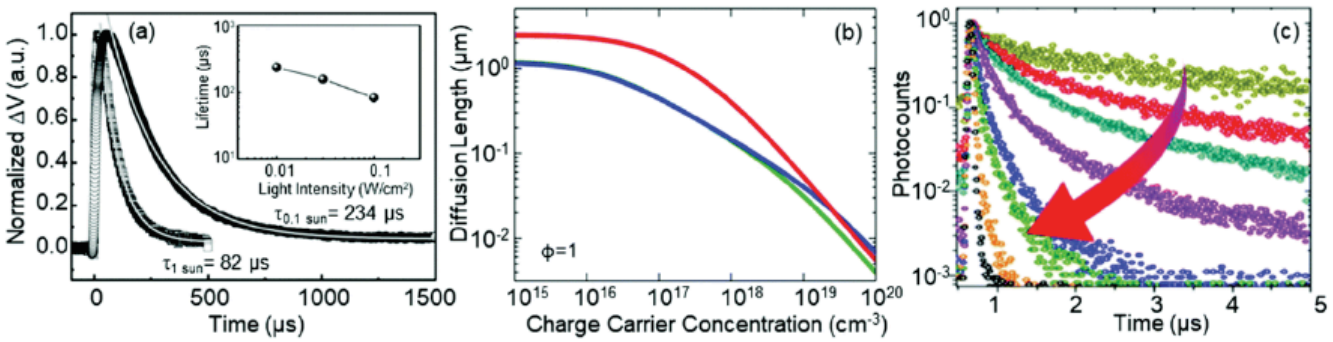

Figure 12: Diagram of the recombination dynamics of charge carriers in perovskite. Ref. [85].

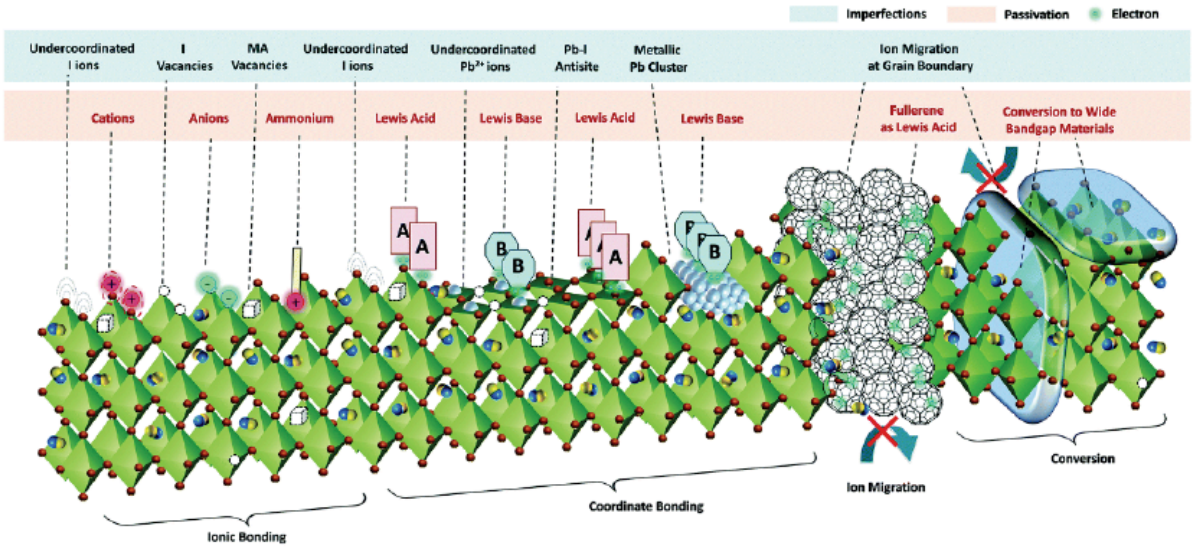

Figure 13: Different types of defects on the surface and grain boundaries of the perovskite film. An example of passivation through ionic bond or coordination bond and converted into wide band gap perovskite is also explained. Ref. [86].

interactions to effectively passivate defects and improve the component and performance stabilities.

3.2.1. Additives Adjusting the Quality of Perovskite Crystals

In additive engineering, various types of additives are used to regulate the growth of perovskite crystals and thin films. The additives can be dissolved in the perovskite precursors and can also be used in the anti-solvent process. Additives include amine or Pb halides, ionic liquids, either inert or active organics (containing polarized functional groups), and other Lewis bases. Xu *et al*. reported the first application of PCBM as a passivation agent added to the perovskite precursor [87]. They found that the hysteresis of the perovskite solar cell with PCBM is significantly reduced, and the carrier recombination is also reduced. The PCBM molecules passivated the $Pb^{-}I$ inversion defects as evidenced by both theory and experiment. Abate *et al*. used iodopentafluorobenzene (IPFB) additives to passivate insufficiently coordinated halide ions [88]. They discovered that the electronic defect nature of the additive made it behave like an electron acceptor, and therefore formed a strong halogen bond with insufficiently coordinated halide or lead halide anti-site defects (Figure **14**). They found that the trap states on the perovskite was fully passivated through the complexation of the supramolecular halogen bond between the additive and the perovskite.

Carvalho *et al*. first used tetraethyl orthosilicate (TEOS) as an additive in the MAI precursor solution during the preparation of the perovskite layer under 50% RH [89]. After MAI reacts with PbI_2, liquid TEOS is evacuated from the growing perovskite lattice, and finally stays at the grain boundary. While the water molecules in the surrounding environment are absorbed by the material, an optical inert SiO_2

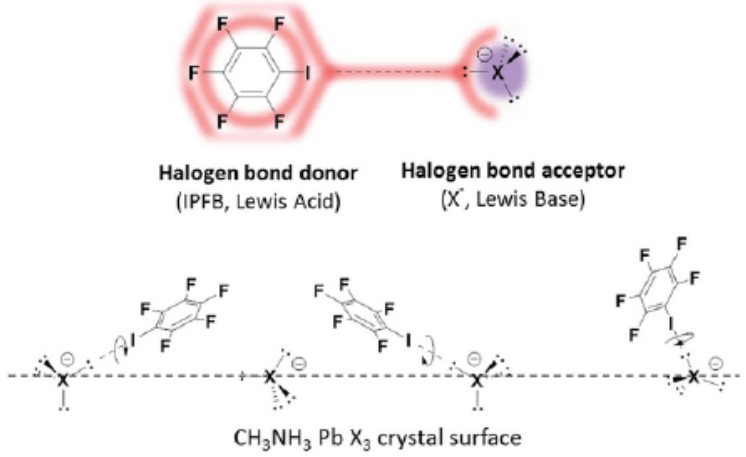

Figure 14: A schematic diagram of the halogen bond interaction between iodopentafluorobenzene as an electron donor and a halogen anion in a perovskite as an electron acceptor. Ref. [88].

passivation layer is formed at the grain boundary, thereby preventing the decomposition of the perovskite. Ye *et al*. report a volatile material that forms a thin, dense interlayer that essentially eliminates the C60-induced nonradiative interfacial recombination loss despite not directly passivating the perovskite surface. The highest PCE is 24.7% by using volatile material [90].

The strength of the interaction between tetrahydrothiophene oxide(THTO) [91] and $MAPbI_3$ is related to the extremely high solubility and exothermal reaction during hydrolysis. Adding THTO to the $MAPbI_3$ precursor solution can significantly reduce the nucleation density. The study found that the crystal orientation of the $MAPbI_3$ film has a significant effect on the open circuit voltage of the solar cell device, which emphasizes the importance of the control the orientation of the (100) crystal plane of the thin film to grow perpendicular to the substrate.

Liu *et al*. greatly improved the quality of the perovskite film by adding methylamine (MA) to the precursor perovskite solution [93]. Their method can also effectively passivate the shallow electron defects that appear in the grain boundaries, thereby prolonging the lifetime of the carriers. Through strong hydrogen bond interaction, the molecular cross-linking effect of MA on the perovskite grains was an important reason for this excellent PSC performance.

Alkylammonium additives can also act as passivators by reacting with the precursors to form smaller-sized perovskite materials [94, 95]. Phenylethylammonium iodide (PEAI) has been used as a defect modifier to benefit PSC, with a maximum PCE of 23.32% [96]. Zheng *et al*. report that the use of surface-anchored alkylamine ligands (AAL) with different chain lengths as grain and interface modifiers can improve grain orientation [97]. The long-chain AAL added to the precursor solution allows significant (100) orientation and reduces the density of trap states, thus highly inhibiting non-radiative recombination and improving the optoelectronic performances of the mixed cation mixed halide perovskite films. As a result, the PCE of the manufactured p-i-n planar PSC reached a record 23%. Jin's group [92] chose long-chain ammonium salt (oleylamine, OA) additives to add perovskite precursors to stabilize the metastable $CsPbI_3$ perovskite structure during film deposition. The study found that the ammonia ligand can selectively stabilize two different perovskite crystal forms, including cubic crystal-$CsPbI_3$ and the distorted orthorhombic crystal-$CsPbI_3$ perovskite structure as shown in Figure **15**. After surface functionalization, the $CsPbI_3$ perovskite film has good photophysical properties and good phase stability.

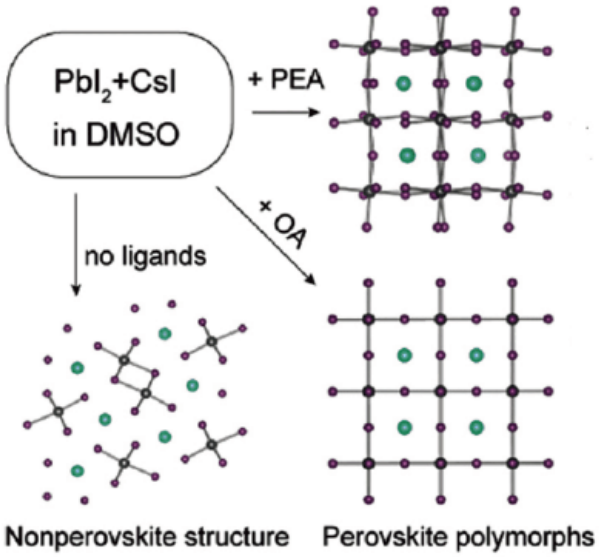

Figure 15: Ammonia ligand selectively stabilizes two different perovskite crystal forms Ref. [92].

Zhao *et al.* used the cationic surfactant n-octyltrimethylammonium bromide OTAB as the perovskite surface modification material to passivate the vacancy and anti-site defects on the surface of the $CH_3NH_3PbI_3$ film [98]. The SCLC and TRPL tests show that the defect state density of the film modified with 0.5 mg mL^{-1} OTAB decreases by more than 70%, and the carrier lifetime doubled. The $CH_3NH_3PbI_3$ layer modified with OTAB can delay the degradation and improve its stability due to its compactness, high uniformity, and hydrophobicity. In the end, the PCE of the perovskite cell modified with OTAB is significantly improved, reaching 18.32%.

Adding non-volatile Lewis base additives into the precursor solution not only increase the uniformity of crystal grains, but also passivate the grain boundaries [136]. With the addition of urea as a Lewis base, the PL lifetime of the resulting perovskite increased. Therefore, PCE also increased due to the reduction of trap-assisted non-radiation recombination. This can be considered as the result of coordination with halogen atoms. Both pyridine and thiophene are Lewis bases, which can form stronger divalent bonds with Pb [137, 138]. Confocal fluorescence microscopy can directly observe the increase in PL quantum yield. After the pyridine vapor treatment, the previously dim particles will become brighter. Not only was the non-radiative recombination reduced within the grain, but also the PL quenching around the grain boundary was weakened. Pyridyl thiourea, etc. can also form adducts with Pb in the precursor solution, delay the growth rate of perovskite crystals, optimize film quality and improve device performance [139]. The efficiency of the perovskite cell modified with 0.5 mg mL^{-1}

2-pyridylthiourea can reach 18.2%, and the stability have been significantly improved. Zhu [140] introduced a carefully designed passivator 4-tert-butylbenzylammonium iodide (tBBAI), whose bulky tert-butyl group prevents unnecessary aggregation through steric repulsion. They showed that the simple surface treatment of tBBAI significantly accelerated the charge extraction of the perovskite into the HTM, and at the same time prevented the non-radiative recombination. This increases the PCE of the PSC to 23.5% and reduces the hysteresis to an almost undetectable level, without carrier recombination. The most apparent improvement was that the FF increased from 0.75 to 0.82 after tBBAI treatment.

Wang *et al*. [99] reported that the perovskiteα-$FAPbI_3$ was successfully applied as a light absorber at a relative humidity of 40%, and the PCE of 16.69% was obtained with fairly high stable. N-methyl-2-pyrrolidone (NMP) as an additive reduce the rate of crystallization by forming FAI:PbI_2:NMP intermediates. During the annealing stage, NMP was separated from the mesophase leading to a simple transformation of the intermediate to α-$FAPbI_3$. This process avoids the indirect delta phase to alpha phase conversion route, which may leave delta phase residues in the film. In a simpler process for manufacturing the $FAPbI_3$ series perovskite type, the photosensitive black phase α-$FAPbI_3$ perovskite must be stable in high humidity. This can be achieved by partially replacing FA with MA or Cs to produce di- or tri-cation perovskites [100].

Abate *et al*. introduced a fullerene derivative used as a Lewis acid additive to adjust the performance of the perovskite surface into a wide band gap material. On the right side of Figure **12** two commonly used passivation methods for such defects are shown.

Liang *et al*. reported that [101] the additives (1,8-diiodooctane, DIO) also promoted nucleation (Figure **16**) and adjusted the kinetics of crystal growth during the crystallization process, resulting in perovskite. The shape became smoother, and crystal uniformity and the coverage area were improved. As a result, they realized planar heterojunction solar cells with PCE up to 12% through a low-temperature solid solution process (below 150°C).

Li *et al*. used the coordination effect of n-electron and π-electron with Pb^{2+} in the molecular structure of benzylacetonitrile (PA) and 2-naphthaleneacetonitrile (2-NA) as a regulator [102]. There was a coordination effect between the regulators and Pb^{2+} in the perovskite precursor solution, which could effectively control the precipitation rate of crystals, promoted crystal growth synergistically, and increased grain size with reduced grain boundaries. The perovskite film prepared by this method more effectively increased the light absorption of the crystal film and the generation of photogenerated carriers. The highest PCE of the mesoporous perovskite solar cell based on the regulation and optimization of benzyl cyanide reached 20.61%.

PMMA is commonly added as an additive to the anti-solvent chlorobenzene, which reduces the free energy barrier of nucleation and promotes the conversion of nucleation mode to rapid heterogeneous nucleation. It induces intermediate adducts formation with lead iodide, which can slow down the growth of crystals. The nucleus adjusts the orientation to reduce the Gibbs free energy, and finally forms a regular oriented perovskite film, with an efficiency of 21.01%, and decrease in density of defect by orders of magnitude [103].

3.2.2. Solvent Engineering and Interface Engineering for Defect Passivation on Surfaces

In order to further obtain high-quality films or crystals, solvent engineering and interface engineering are usually used to improve the performance of PSCs.

Solvent engineering mainly uses solvent vapor or other reagents to reprocess the surface of the perovskite film. For example, Xiao *et al*. used DMF vapor to interact with the perovskite film, thereby slowing down the solvent drying speed, which retarded the growth of crystals or films, resulting in better crystallinity and morphology [104]. It could be directly observed from the cross-sectional SEM photos that the

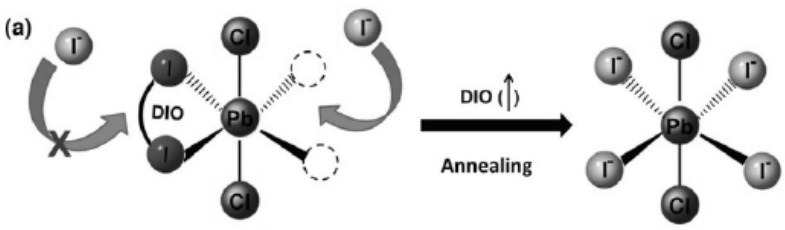

Figure 16: Schematic diagram of transient chelation of Pb^{2+} and DIO [101].

crystallinity was improved, the grain size increases, and the grain boundary formation were greatly suppressed [105]. Because of reducing defects and better crystallinity, photovoltaic cells based on solvent-annealed samples showed up to 15.6% PCE, while the PCE based on thermally annealed samples was only 9.9% [59]. The crystallization regulation and the inhibited defects synergistically enhanced the morphology uniformity and photoelectric properties [106].

In interface engineering, the as-crystallized films are treated with different solvents. For example, the choice of ionic liquid as the interface modifier can protect the perovskite film from degradation. Bai *et al*. added $BMIMBF_4$ ionic liquid, on account of the $BMIM^+$ groups reducing surface defects, leading to an improved long-term thermal and light stability [107]. Yang *et al*. treated the film with guanidine bromide solution to form a large band gap top layer on the original perovskite by secondary growth technology [108]. The non-radiative recombination that led to the reduction of V_{OC} was strongly suppressed on account of the trap passivation of the top layer [109]. Recently, another zwitterionic structure has been discovered, namely 4-(1 H-imidazole-3- ium-3-yl)butane-1-sulfonate (IMS) can be used as a bifunctional deactivator. The sulfonate group of IMS coordinates Pb^{2+} ions and imidazole groups to interact with I^- ions [110], thereby increasing V_{OC} and inhibiting the hysteresis.

Wang *et al*. obtain thermodynamically stable β-$CsPbI_3$ by using choline iodide [111]. Choline iodide fills the pinholes and cracks in the perovskite film, so it can greatly inhibit defect-assisted degradation. The PCE of the solar cell based on $CsPbI_3$ treated with choline iodide was as high as 18.4% at the ambient air temperature of 45±5°C. Peng *et al*. underlined the role of carbonyl (C=O) in passivating Pb^{2+} defects through electron donation [112]. In addition to the above chemical modification, physical modification of the perovskite film can also improve performance. For example, Zhang team [113] developed light processing technology to prepare a $CsPbIBr_2$ photovoltaic film with preferential orientation, high crystallinity, large grain size, full coverage, and high phase purity, as shown in Figure **17**. The growth temperature also has significant influence on the morphology of perovskite. Jia *et al*. introduced a series of organic halide salts with different organic cations and halide anions to control crystallinity and the morphology of perovskite films [114]. When tetrabutylammonium bromide (TBAB) was added to the perovskite ($CsPbI_{2.4}Br_{0.6}$) precursor solution, the UV-vis absorption remained the same as before. Simultaneously, they obtain larger grain size and higher crystallinity samples and excellent charge transport performance. The PSC showed a 15.21% PCE, while still maintaining over 93% of its initial PCE when stored in N_2 for 1600 hours. Under thermal annealing, organic cations can evaporate, leaving excess BX_2 (such as PbI_2) to passivate the surface, which is called the "self-passivation" effect [115]. At a fixed temperature of 150°C, increasing the time from 5 minutes to 100 minutes could reduce the defect density, resulting in hysteresis suppression as exampled by a solar cell based on $FA_{0.9}Cs_{0.1}PbI_3$ [116].

4. APPLICATION OF PEROVSKITE

4.1. In Perovskite Solar Cells

Perovskite is a promising solar cell material due to their high absorption coefficient, long carrier diffusion length, high defect tolerance and low exciton binding energy. The quality of the perovskite layer and the less defective interfaces are important for a highly efficient PSC. Various device manufacturing technologies and optimization of hole and electron transport processes contribute to the rapid development of PSC. For instance, Spiccia and colleagues [117] obtained the PCE of 13.9% by using a microcrystalline $MAPbI_3$ perovskite film that is without grain boundaries. Then, the PCE was increased to greater than 15% for the mixture of $MAPbI_3$ and $MAPbI_{3-x}Cl_x$ perovskite [105], to over 20% for $MAPbI_3$ perovskite by blade coating method, over 23% for the recipe of mixed cation (MA/FA) and mixed halogenation (I/Br) [118]. The following Figure **18** and **19** shows respective layer and energy level diagrams of the regular or inverted perovskite solar cells [85, 119]. Compared with the regular devices, the inverted pattern demonstrates several advantages of less hysteresis, less demand of

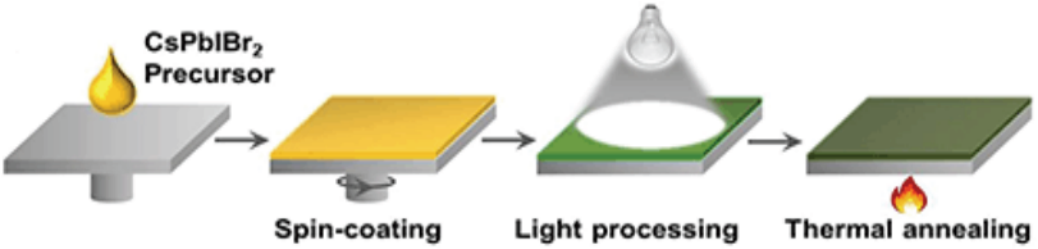

Figure 17: Light-processing method. Reprinted with permission from Ref. [113].

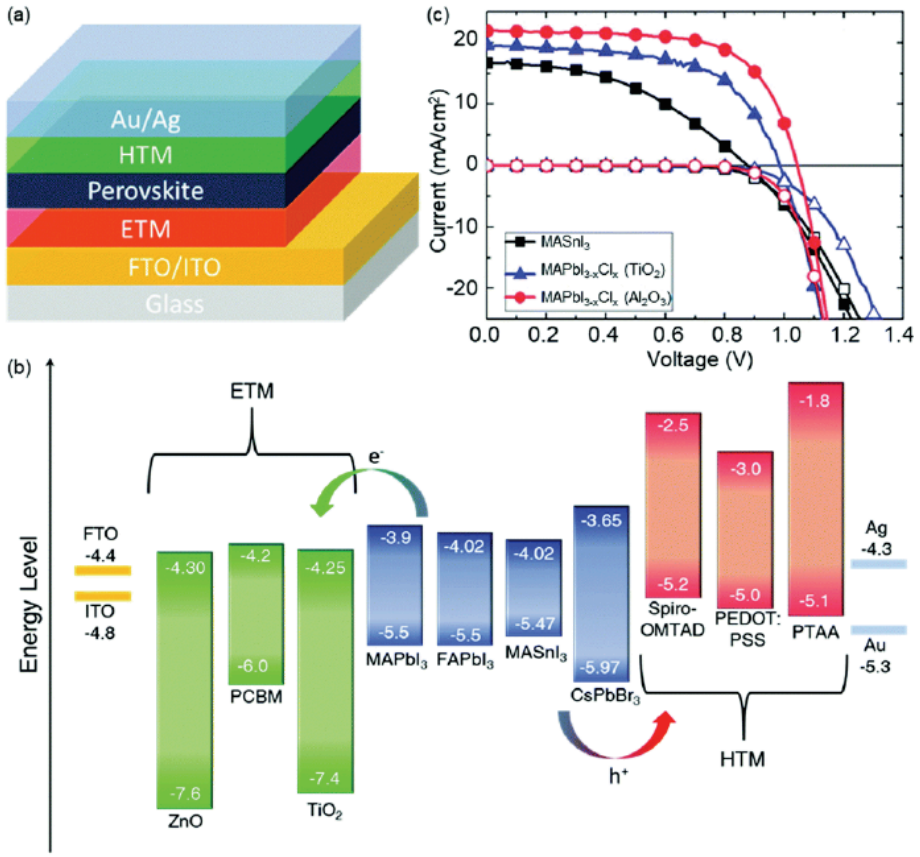

Figure 18: Regular perovskite solar cells. (**a**) PSC device stacking architecture. (**b**) The energy levels of typical electron transport, hole transport, perovskite and electrode materials. (**c**) Current-voltage curves of lead and tin-based PSCs. Ref. [85].

hole transport layer thickness with less internal resistance, and the inexpensive Ag or Cu instead of Au for the regular one [120]. Since 2023, even the PCE performance of inverted PSC was first reported to surpassed the regular one, benefited from self-assembled hole-selective molecules outperforming the synergistic role of dopant and buried interface (ITO/perovskite) modification [121]. This decisive victory started to attract dominant research on the inverted device, especially on similar self-assembled molecular (SAM) design with more functional groups for inducing the wettability and crystallinity with the upper perovskite precursor [122]. Khulud. *et al*. even succeeded in inducing better single crystal growth by MeO-2PACz SAM and achieved a high PCE of 23.1% and obviously prolonged operational stability compared to that based-on PTAA HTL, setting a new benchmark for single-crystal perovskite solar cells [123].

4.2. In Quantum-Dot Light-Emitting Diodes

The adjustable PL emission peak and high photoluminescence quantum yield (PLQY) of perovskite have attracted researcher to manufacture multicolor perovskite LEDs (PeLED. Recently, the (peak) external quantum efficiency (EQE) of the blue (26.4%) [124], green (31%) [125] and red (32.14%) [126] PeLEDs have been greatly improved.

The stability and efficiency of PeLED are affected by crystal structures, temperature, light, and atmosphere. By selecting the appropriate electron and hole transport layer and modifying their interfaces with perovskite active layer, a balanced charge injection and transport can be achieved, and the current in the perovskite layer can also be increased by ameliorating the surface coverage and reducing the surface roughness. Another important factor in achieving high performance PeLED is suppressing non-radiative recombination. For example, a 20.3% EQE and 80% PLQY PeLED device/MABr perovskite layer was fabricated using the graded quasi-core/shell $CsPbBr_3$ [127].

The brominated compound $MAPbBr_3$ has a band gap of approximately 2.3 eV and has been selected as the green candidate for visible laser and luminescence applications [128]. The indicator of PLQY is important for these two applications. Sasol's team invented a new doping method [129] to produce high PLQY perovskite-based materials, in which stable alumina nanoparticles (NPs) were mixed into the perovskite precursor. The substrate was spin-coated in air to prepare perovskite film, and then annealed at 90℃ for 1 h. The concentration and size of Al_2O_3 NPs together determined the size of the nanocrystals. It showed that

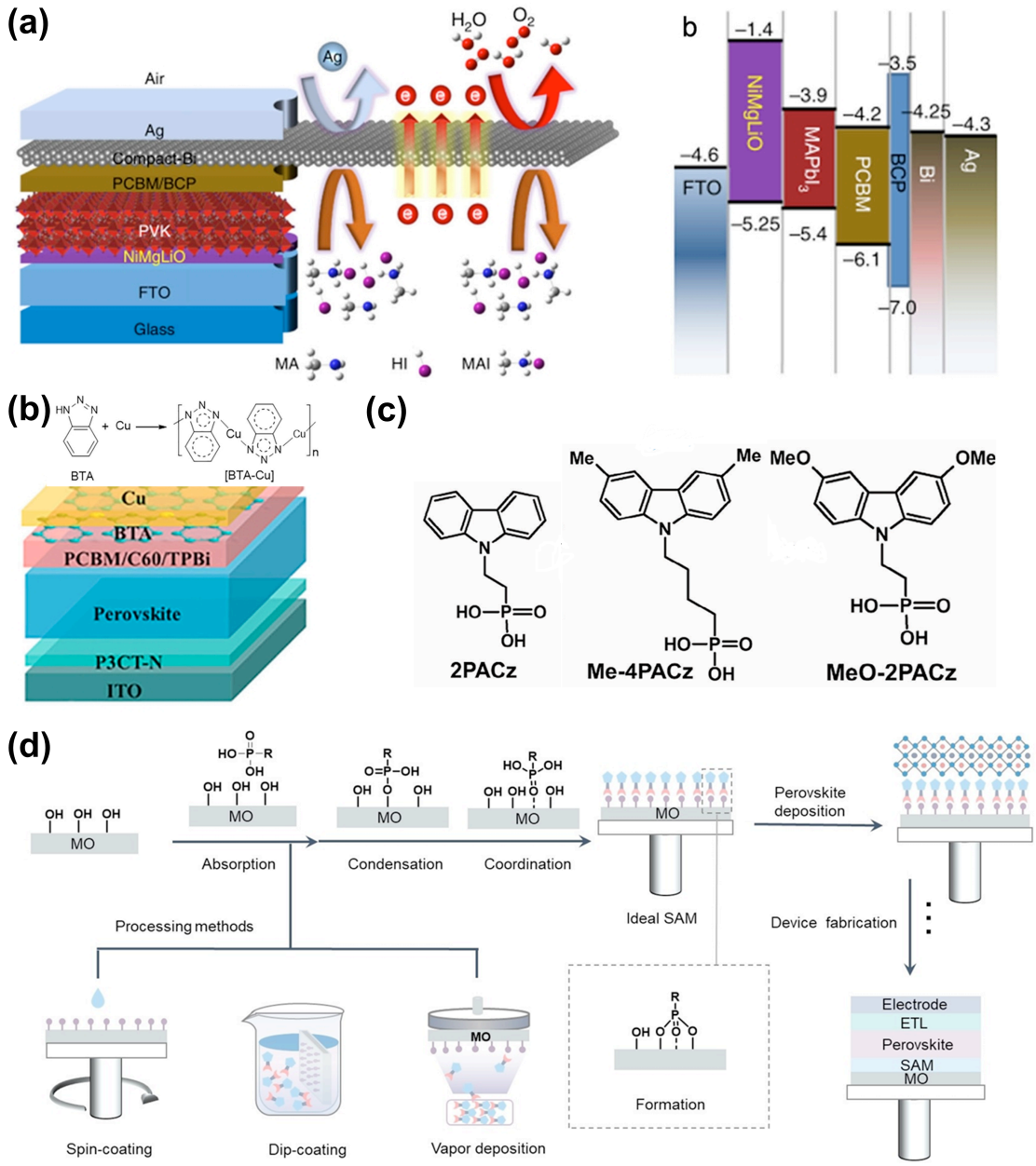

Figure 19: Inverted perovskite solar cells. (**a**) PSC device stacking architecture with an additional protecting layer for suppression of interfacial ion migration as well as external species isolation, and relative energy level structures of each layer. (**b**) cost-effective Cu electrode and its partner BTA for interface stabilization [119]. (**c**) Currently used commercial SAM molecules and (**d**) schematics of SAMs bonding on either ITO substrate or typical NiO_x HTLs during mild thermal treatment and the adoptable processing methods [122].

the self-assembly of Al_2O_3 NPs limited the growth of perovskite at the nanometer scale and spontaneously formed isotropic $MAPbBr_3$ nanocrystals. The photoluminescence was strongly enhanced. In addition, the material was not sensitive to moisture and could be easily processed in solution, which made it a practical material for applications in the field of luminescence and lasers.

4.3. In Photodetectors

Photodetector can convert light to electrical signals and has been widely used in fields such as imaging, environmental monitoring, missile early warning, and biological detection. The most attractive feature of perovskites is their high sensitivity to visible light and high photovoltage. In recent years, these excellent properties of perovskite have been greatly explored in photodetectors. The emergence of perovskite (especially single crystal perovskite) semiconductor materials is expected to bring a huge breakthrough both on the cost and sensing performances.

Zhao's team fabricated a simple capillary system to enable the growth of single crystal microstrip arrays (MRAs) directly from the perovskite precursor solution. The 100-day constant stress test was carried out under the conditions of 450 nm illumination in the

environment, and the produced photodetector maintained 90% performance and good operational stability. Yan's team fabricated a planar photodetector on the (100) face of $MAPbI_3$ single crystal. Due to the low trap density and excellent charge transport performance of the single crystal surface, this photodetector has a higher gain [131]. This kind of detector has a responsivity of 1×10^{3} $A\cdot W^{-1}$, and a fast response speed of 132 μs. Compared with the corresponding photodetector based on $MAPbI_3$ polycrystalline film, the responsivity and EQE are both improved by about two orders of magnitude, and the response speed is accelerated by 3 times. In addition, the detector has good stability and can be placed in the atmosphere for up to 40 days. Small noise current and low noise equivalent power (NEP) value are the prerequisites for preparing highly sensitive photodetectors. Liu's team fabricated about 100 photodetectors on a 150 μm thick $MAPbI_3$ single crystal perovskite wafer [132]. This work demonstrated for the first time the feasibility of mass production of integrated circuits on ultra-thin single crystal wafers. The photocurrent of this photodetector can reach 700 μA under a bias of 2 V, which is 350 times higher than that of a polycrystalline thin film photodetector based on the same material. ZnO NPs were introduced into the precursor solution of $CsPbBr_3$ to obtain a thin film with more uniform and compact particle distribution. $CsPbBr_3$ and $CsPbBr_3$: ZnO precursors need to be prepared in a N_2 glove box. Adding ZnO NPs to the $CsPbBr_3$ precursor can form a $CsPbBr_3$:ZnO precursor solution at 60°C for 30 min. Therefore, the preparation of $CsPbBr_3$ and $CsPbBr_3$:ZnO thin films introduces the spinning coating process. In order to wash away the solvent on the wet perovskite film, 1 ml of chlorobenzene needs to be transferred to the wafer within 15 seconds of spin coating [54]. The annealing process removes the residual DMSO solvent. The performance of the photodetector prepared with all inorganic $CsPbBr_3$: ZnO is better than that of the photodetector without doping ZnO [133].

4.4. In Photocatalysis

To mimic the natural photosynthesis procedure fixing CO_2, it has set off a research boom in the photocatalytic reduction of CO_2 [134, 135]. Photocatalysis and photovoltaic technology are the two most feasible ways to utilize solar energy. Photocatalysis can directly convert energy in the form of chemical endothermal reactions, and it plays a vital role in clean energy production. While the photovoltaic series or modules can provide enough voltage to drive such energy storage reactions. In addition to focusing on perovskite modification (such as crystallization and defect engineering), a new PEC system for water splitting, which is the prerequisite for final CO_2 reduction is also proposed, which integrates the concept of photovoltaic. An electrode with efficient electron-hole pair separation, faster charge transfer and higher stability can be achieved, which also calls for the previous experiences on perovskite engineering.

Xu *et al*. [18] reported the application of halide perovskite $CsPbBr_3$ QDs. This method uses artificial photosynthesis of $CsPbBr_3$ / GO to convert photocatalytic reduction of CO_2 into ethyl acetate, which is full use of visible light. In addition, the size of the halide perovskite controls the process of CO_2 conversion. The smaller $CsPbBr_3$ QD has a narrower band gap, the 8.5 nm size $CsPbBr_3$ QD has the longest photoluminescence lifetime, and the CO_2 reduction product yield is the highest. Due to its soft polarity and the 7-fold increase in the solubility of CO_2, ethyl acetate is introduced to stabilize $CsPbBr_3$ [19, 20]. This provides a strong basis for the in-depth study of the use of CO_2 by halogenated perovskites. In 2019, it was reported that 2D MXene has a similar effect to GO, and its CO and CH_4 formation rates were 26.32 and 7.25 $\mu mol\ g^{-1}\ h^{-1}$, respectively [21].

5. CONCLUSIONS AND PROSPECTS

In summary, we reviewed the development and the promising prospect of the organic-inorganic halide perovskite materials and film engineering for solar cells, OLEDs and photodetectors, etc. The optoelectronic properties depend to a large extent on the composition of the halide as well as the high crystallinity. Their light absorption and emission colors from visible light to near infrared region are achieved through the synthesis of pure or alloyed halide perovskites. In addition, these properties can be adjusted by changing the temperature, the pressure, the composition of the A site/halide ions, or controlling the size and shape of the crystal. The easy generation and long-distance diffusion of the free carriers make itself smooth in charge separation in solar cells and photodetectors. Perovskite are also used in high-efficiency multicolor LEDs and low-threshold lasers because of its tunable emission wavelength by simple quantum size effect and high-yield photoluminescence quantum.

Although perovskite materials show excellent photoelectric properties and devices, they are toxic and environmentally unfriendly, encouraging researchers to develop lead-free perovskite materials. The poor stability of perovskite to moisture and oxygen is another critical challenge. The stability related to crystallinity and defect density can be a considerable limiting factor for perovskite devices. At present, the life span of the prepared device in the surrounding environment is far below the market standard and the

perovskite halide materials needs to be significantly stabilized under environmental light, air, moisture, and temperature. The most vulnerable areas are surfaces, interfaces, and grain boundaries. Therefore, it is very important to passivate surface defects and grain boundaries. New HTL and ETL, passivation layer, additive engineering, solvent and thermal annealing have been applied to suppress the defect state generation or passivate the existing defects. These include relative passivation mechanisms on supplement of unsaturated coordination between Lewis acid-base functional groups, hydrogen bonding, electrostatic attraction, hydrophobic protective layer or framework, etc. Sometimes, only reduced defect density and high stability may not guarantee higher photoelectric conversion efficiency, the band alignment principle is also another issue to minimize the charge transport loss, which is beyond this topic. Researchers need to strive for simultaneous perovskite stabilization and interface energy level matching, both for high performances and good stability. More innovative optimization strategy towards the crystallization and interface passivation are expected, especially beyond the typical noncovalent interactions.

This review introduces the basic structure and properties of perovskite materials, as well as the preparation methods of single crystal and thin film with better quality. The way of preparing thin film with large grain, little grain boundary and greatly inhibited defects, would cater the wide application of perovskite in various fields. In short, we hoped that all the perovskite devices would proceed to turn more efficient, stable, eco-friendly, cheap and recyclable enough for commercialization as soon as possible, along with the new ideas of those engaged in this magnificent target.

CONFLICTS OF INTEREST

There are no conflicts of interest to declare

ACKNOWLEDGEMENTS

This work was supported by the National Key Research and Development Program of China (2021YFB3800101) and Natural Science Foundation of China (No. 22178257).

REFERENCE

[1] Korshunova K, Winterfeld L, Beenken W, raunge E. Thermodynamic stability of mixed Pb:Sn methyl-ammonium halide perovskites. Physica Status Solidi (B) Basic Research 2016, 253: 1907-1915 https://doi.org/10.1002/pssb.201600136

[2] Li C, Ding W, Feng L, Gao Y. Formability of ABX_3 (X = F, Cl, Br, I) halide perovskites. Acta Crystallographica Section B: Structural Science 2008, 64: 702-707 https://doi.org/10.1107/S0108768108032734

[3] Wang K, Yang D, Wu C. Recent progress in fundamental understanding of halide perovskite semiconductors. Progress in Materials Science 2019, 106: 100580 https://doi.org/10.1016/j.pmatsci.2019.100580

[4] Gao Y, Song Z, Fu Q, Controlled Nucleation and Oriented Crystallization of Methylammonium-Free Perovskites via In Situ Generated 2D Perovskite Phases. Advanced Materials 2024, 36: 2405921 https://doi.org/10.1002/adma.202405921

[5] Zhu HW, Liu YH. Tailored Amphiphilic Molecular Mitigators for Stable Perovskite Solar Cells with 23.5% Efficiency. Advanced Materials. 2020, 32: 1-8 https://doi.org/10.1002/adma.201907757

[6] Liu Y, Yang Z, Cui Y. Two-Inch-Sized Perovskite $CH3NH3PbX_3$ (X = Cl, Br, I) Crystals: Growth and Characterization. Advanced Materials. 2015, 27: 5176-5183 https://doi.org/10.1002/adma.201502597

[7] Chen S, Dai X, Xu S, Jiao H, Zhao L, J. Huang. Stabilizing perovskite-substrate interfaces for high-performance perovskite modules. Science 2021, 373: 902 https://doi.org/10.1126/science.abi6323

[8] Feng W, Tao J, Liu G, Yang G, Zhong JX, Angew. Chem., Int. Ed. 2023, 62: 202300265 https://doi.org/10.1002/anie.202300265

[9] Alcocer MJ P, Leijtens T. Electron-Hole Diffusion Lengths Exceeding Trihalide Perovskite Absorber. Science 2013, 342: 341-344 https://doi.org/10.1126/science.1243982

[10] Chen H,Ye F. A solvent-and vacuum-free route to large-area perovskite films for efficient solar modules. Nature. 2017, 550: 92-95 https://doi.org/10.1038/nature23877

[11] Li M, Zhao C. Interface Modification by Ionic Liquid: A Promising Candidate for Indoor Light Harvesting and Stability Improvement of Planar Perovskite Solar Cells. Advanced Energy Materials. 2018, 8: 1801509 https://doi.org/10.1002/aenm.201801509

[12] Wang Y, Chen W. Dopant-Free Small-Molecule Hole-Transporting Material for Inverted Perovskite Solar Cells with Efficiency Exceeding 21%. Advanced Materials. 2019, 31: 1-10 https://doi.org/10.1002/adma.201902781

[13] Quan, L. N., García de Arquer, F. P. Perovskites for Light Emission. Advanced Materials. 2018, 30: 1-19 https://doi.org/10.1002/adma.201801996

[14] Cao Y, Wang N. Structures. Nature (2018).

[15] Tian W, Zhou H. Hybrid Organic-Inorganic Perovskite Photodetectors. Small. 2017, 13: 1702107 https://doi.org/10.1002/smll.201702107

[16] Zhang X, Dong X. A Self-Powered Photodetector Based on Polarization-Driven in CH3NH3PbI3 Single Crystal (100) Plane. Chemical Engineering Journal 125957 (2020). https://doi.org/10.1016/j.cej.2020.125957

[17] Chen J, Du W. Perovskite quantum dot lasers. InfoMat. 2020, 2: 170-183 https://doi.org/10.1002/inf2.12051

[18] Xu YF, Yang M. A CsPbBr3 Perovskite Quantum Dot/Graphene Oxide Composite for Photocatalytic CO_2 Reduction. Journal of the American Chemical Society. 2017, 139: 5660-5663 https://doi.org/10.1021/jacs.7b00489

[19] Zhu X, Lin Y. Lead halide perovskites for photocatalytic organic synthesis. Nature Communications. 2019, 10: 1-10 https://doi.org/10.1038/s41467-019-10634-x

[20] Wang, T, Zeng, G, Yang, YM. Advances in Metal Halide Perovskite Scintillators for X-Ray Detection. Nano-Micro Lett. 2025,17: 275 https://doi.org/10.1007/s40820-025-01772-7

[21] Pan A, Ma X. $CsPbBr_3$ Perovskite Nanocrystal Grown on MXene Nanosheets for Enhanced Photoelectric Detection and Photocatalytic CO_2 Reduction. Journal of Physical Chemistry Letters. 2019, 10: 6590-6597 https://doi.org/10.1021/acs.jpclett.9b02605

[22] Song X, Hu J, Zeng H. Two-dimensional semiconductors: Recent progress and future perspectives. Journal of Materials Chemistry C. 2013, 1: 2952-2969 https://doi.org/10.1039/c3tc00710c

[23] Wang X, Ling Y. Dynamic Electronic Junctions in Organic-Inorganic Hybrid Perovskites. Nano Letters. 2017, 17: 4831-4839 https://doi.org/10.1021/acs.nanolett.7b01665

[24] Ha ST, Liu X. Synthesis of Organic-Inorganic Lead Halide Perovskite Nanoplatelets: Towards High-Performance Perovskite Solar Cells and Optoelectronic Devices. Advanced Optical Materials. 2014, 2: 838-844 https://doi.org/10.1002/adom.201400106

[25] Mao L, Stoumpos CC, Kanatzidis MG. Two-Dimensional Hybrid Halide Perovskites: Principles and Promises. Journal of the American Chemical Society. 2019, 141: 1171-1190 https://doi.org/10.1021/jacs.8b10851

[26] Krishna A, Gottis S. Mixed Dimensional 2D/3D Hybrid Perovskite Absorbers: The Future of Perovskite Solar Cells? Advanced Functional Materials. 2019, 29: 1-20 https://doi.org/10.1002/adfm.201806482

[27] Tsai, H. *et al*. High-efficiency two-dimensional ruddlesden-popper perovskite solar cells. Nature. 2016, 536:312-316 https://doi.org/10.1038/nature18306

[28] Yuan, C. L.; Zhang, Z. T.; Tang, S. Y.; Gou, Y. S.; Zhao, P.; Li, H. M.; Yu, H., Cooperation of Dual Organic Spacers and A Site Cations for High-Performance Quasi-2D Ruddlesden-Popper Perovskite Solar Cells. Chempluschem 2025. https://doi.org/10.1002/cplu.202500169

[29] Zhang, F.; Lu, H. P.; Tong, J. H.; Berry, J. J.; Beard, M. C.; Zhu, K., Advances in two-dimensional organic-inorganic hybrid perovskites. Energy & Environmental Science 2020, 13 (4): 1154-1186. https://doi.org/10.1039/C9EE03757H

[30] Wu, Y. *et al*. In Situ Passivation of $PbBr_{64}$- Octahedra toward Blue Luminescent $CsPbBr_3$ Nanoplatelets with Near 100% Absolute Quantum Yield. ACS Energy Letters. 2018, 3: 2030-2037 https://doi.org/10.1021/acsenergylett.8b01025

[31] Spina M, Lehmann M. Microengineered $CH_3NH_3PbI_3$ Nanowire/Graphene Phototransistor for Low-Intensity Light Detection at Room Temperature. Smal.l 2015, 11: 4824-4828 https://doi.org/10.1002/smll.201501257

[32] Chang PH, Liu S. Ultrahigh responsivity and detectivity graphene-perovskite hybrid phototransistors by sequential vapor deposition. Scientific Reports. 2017, 7: 1-10 https://doi.org/10.1038/srep46281

[33] Cheng HC,Wang G. Van der Waals Heterojunction Devices Based on Organohalide Perovskites and Two-Dimensional Materials. Nano Letters. 2016, 16: 367-373 https://doi.org/10.1021/acs.nanolett.5b03944

[34] Dong Q, Fang Y. Electron-hole diffusion lengths > 175 m m in solution-grown $CH_3NH_3PbI_3$ single crystals. Science. 2015, 347: 967-970 https://doi.org/10.1126/science.aaa5760

[35] Zhou H, Nie Z. Antisolvent diffusion-induced growth, equilibrium behaviours in aqueous solution and optical properties of $CH_3NH_3PbI_3$ single crystals for photovoltaic applications. RSC Advances. 2015, 5: 85344-85349 https://doi.org/10.1039/C5RA17579H

[36] Liu Y, Ren X. 120 Mm Single-Crystalline Perovskite and Wafers: Towards Viable Applications. Science China Chemistry. 2017, 60: 1367-1376 https://doi.org/10.1007/s11426-017-9081-3

[37] Dang Y, Ju D, Wang L. Recent progress in the synthesis of hybrid halide perovskite single crystals. CrystEngComm. 2016, 18: 4476-4484 https://doi.org/10.1039/C6CE00655H

[38] Yang Z, Deng Y. High-Performance Single-Crystalline Perovskite Thin-Film Photodetector. Advanced Materials. 2018, 30: 1-7 https://doi.org/10.1002/adma.201704333

[39] Bi C, Wang Y. Non-wetting surface-driven high-aspect-ratio crystalline grain growth for efficient hybrid perovskite solar cells. Nature Communications. 2015, 6: 1-7 https://doi.org/10.1038/ncomms8747

[40] Dirin DN, Cherniukh I, Yakunin S. Solution-Grown CsPbBr3Perovskite Single Crystals for Photon Detection. Chemistry of Material.s 2016, 28: 8470-8474 https://doi.org/10.1021/acs.chemmater.6b04298

[41] Peng W, Wang L. Solution-Grown Monocrystalline Hybrid Perovskite Films for Hole-Transporter-Free Solar Cells. Advanced Materials. 2016, 28: 3383-3390 https://doi.org/10.1002/adma.201506292

[42] Zhumekenov AA, Burlakov M. The Role of Surface Tension in the Crystallization of Metal Halide Perovskites. ACS Energy Letters 2, 1782-1788 (2017). https://doi.org/10.1021/acsenergylett.7b00468

[43] Yao Z, Yang Z. Local temperature reduction induced crystallization of $MASnI_3$ and achieving a direct wafer production. RSC Advances. 2017, 7: 38155-38159 https://doi.org/10.1039/C7RA07101A

[44] Wang Q, Lin F. Enhancing efficiency of perovskite solar cells by reducing defects through imidazolium cation incorporation. Materials Today Energy. 2018, 7: 161-168 https://doi.org/10.1016/j.mtener.2017.09.007

[45] Gupta R, Korukonda T. Room temperature synthesis of perovskite ($MAPbI_3$) single crystal by anti-solvent assisted inverse temperature crystallization method. Journal of Crystal Growth. 2020, 537: 125598 https://doi.org/10.1016/j.jcrysgro.2020.125598

[46] Tidhar Y, Edri E. Crystallization of methyl ammonium lead halide perovskites: Implications for photovoltaic applications. Journal of the American Chemical Society. 2014, 136: 13249-13256 https://doi.org/10.1021/ja505556s

[47] Shi D, Adinolfi V. Low trap-state density and long carrier diffusion in organolead trihalide perovskite single crystals. Science. 2015, 347: 519-522 https://doi.org/10.1126/science.aaa2725

[48] Yu W, Li F. Single crystal hybrid perovskite field-effect transistors. Nature Communications. 2018, 9: 1-10 https://doi.org/10.1038/s41467-018-07706-9

[49] Zhang, X. L.; Huang, H. H.; Zhao, C. Y.; Yuan, J. Y., Surface chemistry-engineered perovskite quantum dot photovoltaics. Chemical Society Reviews 2025, 54 (6): 3017-3060. https://doi.org/10.1039/D4CS01107D

[50] Chen, Z. A.; Li, H. T.; Yuan, C. X.; Gao, P. L.; Su, Q.; Chen, S. M., Color Revolution: Prospects and Challenges of Quantum-Dot Light-Emitting Diode Display Technologies. Small Methods 2024, 8 (2): 202300359. https://doi.org/10.1002/smtd.202300359

[51] Choi, D.; Kim, H.; Bae, Y.; Lim, S.; Park, T., Perovskite Colloidal Quantum Dots with Tailored Properties: Synthesis Strategies and Photovoltaic Applications. Acs Energy Letters 2024, 9 (6): 2633-2658. https://doi.org/10.1021/acsenergylett.4c00632

[52] Qin, Z. P.; Wang, S. R.; Zhu, Y. L.; Yuan, L. F.; Zhang, X. Y.; Li, X. G.; Liu, H. L., Co-regulation strategy dominated by double short molecules permitting the regrowth of quantum dots for efficient deep-blue perovskite light-emitting diodes. Nano Energy 2024, 121: 109263. https://doi.org/10.1016/j.nanoen.2024.109263

[53] Zhou, J.; Liu, H. L.; Wang, S. S.; Yuan, L. F.; Dridi, N.; Wang, S. R.; Mattoussi, H.; Li, X. G., Ca^{2+} induced highly fluorescent $CsPb(Br/Cl)_3$ perovskite quantum dots via fast Anion-Exchange & Cation-Doping Inter-Promotion strategy for efficient deep-blue light-emitting diodes. Chemical Engineering Journal 2024, 489: 151227. https://doi.org/10.1016/j.cej.2024.151227

[54] Zhang X, Wang W. Thin film perovskite light-emitting diode based on $CsPbBr_3$ powders and interfacial engineering. Nano Energy. 2017, 37: 40-45 https://doi.org/10.1016/j.nanoen.2017.05.005

[55] Pascoe AR, Gu Q. Directing nucleation and growth kinetics in solution-processed hybrid perovskite thin-films. Science

China Materials. 2017, 60: 617-628
https://doi.org/10.1007/s40843-017-9043-y

[56] Zhou Y, Game OS. Microstructures of Organometal Trihalide Perovskites for Solar Cells: Their Evolution from Solutions and Characterization. Journal of Physical Chemistry Letters. 2015, 6: 4827-4839
https://doi.org/10.1021/acs.jpclett.5b01843

[57] Lamer VK, Dinegar RH. Theory, Production and Mechanism of Formation of Monodispersed Hydrosols. Journal of the American Chemical Society.1950, 72: 4847-4854
https://doi.org/10.1021/ja01167a001

[58] Huang F, LiM. From scalable solution fabrication of perovskite films towards commercialization of solar cells. Energy and Environmental Science. 2019, 12: 518-549.
https://doi.org/10.1039/C8EE03025A

[59] Eperon GE, Burlakov VM. Morphological control for high performance, solution-processed planar heterojunction perovskite solar cells. Advanced Functional Materials. 2014, 24: 151-157
https://doi.org/10.1002/adfm.201302090

[60] Zhang Y, Liu Y. Perovskite $CH_3NH_3Pb(Br_xI_{1-x})_3$ single crystals with controlled composition for fine-tuned bandgap towards optimized optoelectronic applications. Journal of Materials Chemistry C. 2016, 4: 9172-9178
https://doi.org/10.1039/C6TC03592B

[61] Guo Y, Yin X, Liu J. Highly efficient $CsPbIBr_2$ perovskite solar cells with efficiency over 9.8% fabricated using a preheating-assisted spin-coating method. Journal of Materials Chemistry A. 2019, 7: 19008-19016
https://doi.org/10.1039/C9TA03336J

[62] Murali B, Saidaminov M. Robust and air-stable sandwiched organo-lead halide perovskites for photodetector applications. Journal of Materials Chemistry C. 2016, 4: 2545-2552
https://doi.org/10.1039/C6TC00610H

[63] Liu X, Tian X. Boosting the efficiency of carbon-based planar $CsPbBr_3$ perovskite solar cells by a modified multistep spin-coating technique and interface engineering. Nano Energy. 2019, 56: 184-195
https://doi.org/10.1016/j.nanoen.2018.11.053

[64] Bu, T. L.; Ono, L. K.; Li, J.; Su, J.; Tong, G. Q.; Zhang, W.; Liu, Y. Q.; Zhang, J. H.; Chang, J. J.; Kazaoui, S.; Huang, F. Z.; Cheng, Y. B.; Qi, Y. B., Modulating crystal growth of formamidinium-caesium perovskites for over 200 cm^2 photovoltaic sub-modules. Nature Energy 2022, 7 (6): 528-536.
https://doi.org/10.1038/s41560-022-01039-0

[65] Burgués-Ceballos I, Stella M. Towards industrialization of polymer solar cells: Material processing for upscaling. Journal of Materials Chemistry A. 2014, 2: 17711-17722
https://doi.org/10.1039/C4TA03780D

[66] Ge X, Huang Z, Gao Y, Liu Z, Shi B, Zhang XD, Electronic Homogenization Regulation via Nicotinamide Derivative Ligands for Efficient Blade-Coated Wide-Bandgap Perovskite Solar Cells. Adv. Funct. Mater. 2025: 2503504
https://doi.org/10.1002/adfm.202503504

[67] Ma, M. G.; Zhang, C. L.; Ma, Y. J.; Li, W. L.; Wang, Y.; Wu, S. H.; Liu, C.; Mai, Y. H., Efficient and Stable Perovskite Solar Cells and Modules Enabled by Tailoring Additive Distribution According to the Film Growth Dynamics. Nano-Micro Letters 2025, 17 (1).
https://doi.org/10.1007/s40820-024-01538-7

[68] Mohamad Noh MF, Arzaee N. High-humidity processed perovskite solar cells. Journal of Materials Chemistry A. 2020, 8: 10481-10518
https://doi.org/10.1039/D0TA01178A

[69] Gao H, Bao C. Nucleation and crystal growth of organic-inorganic lead halide perovskites under different relative humidity. ACS Applied Materials and Interfaces. 2015, 7: 9110-9117
https://doi.org/10.1021/acsami.5b00895

[70] Wang F, Zhang T. Steering the crystallization of perovskites for high-performance solar cells in ambient air. Journal of Materials Chemistry A. 2019, 7: 12166-12175
https://doi.org/10.1039/C9TA02566A

[71] Kim JH, Williams ST. Enhanced Environmental Stability of Planar Heterojunction Perovskite Solar Cells Based on Blade-Coating. Advanced Energy Materials. 2015, 5: 1401229
https://doi.org/10.1002/aenm.201401229

[72] Wang Q, Eslamian M. Achieving fully blade-coated ambient-processed perovskite solar cells by controlling the blade-coater temperature. IEEE Journal of Photovoltaics. 2018, 8: 1662-1669
https://doi.org/10.1109/JPHOTOV.2018.2861752

[73] Deng Y, Zheng X. Surfactant-controlled ink drying enables high-speed deposition of perovskite films for efficient photovoltaic modules. Nature Energy. 2018, 3: 560-566
https://doi.org/10.1038/s41560-018-0153-9

[74] Li J, Munir R. Phase Transition Control for High-Performance Blade-Coated Perovskite Solar Cells. Joule. 2018, 2: 1313-1330
https://doi.org/10.1016/j.joule.2018.04.011

[75] Hariz, A. Perspectives on organolead halide perovskite photovoltaics. Journal of Photonics for Energy. 2016 6: 032001
https://doi.org/10.1117/1.JPE.6.032001

[76] Mitzi DB, Prikas MT, Chondroudis K. Thin film deposition of organic-inorganic hybrid materials using a single source thermal ablation technique. Chemistry of Materials. 1999, 11: 542-544
https://doi.org/10.1021/cm9811139

[77] Liu M, Johnston MB, Snaith HJ. Efficient planar heterojunction perovskite solar cells by vapour deposition. Nature. 2013, 501: 395-398
https://doi.org/10.1038/nature12509

[78] Liu Z, Li Y. One-Step Vapor-Phase Synthesis and Quantum-Confined Exciton in Single-Crystal Platelets of Hybrid Halide Perovskites. Journal of Physical Chemistry Letters. 2019, 10: 2363-2371
https://doi.org/10.1021/acs.jpclett.9b00777

[79] Mi Y, Liu Z. Fabry-Pérot Oscillation and Room Temperature Lasing in Perovskite Cube-Corner Pyramid Cavities. Small. 2018, 14:1-8
https://doi.org/10.1002/smll.201703136

[80] Chen J, Fu Y. Vapor-Phase Epitaxial Growth of Aligned Nanowire Networks of Cesium Lead Halide Perovskites ($CsPbX_3$, X = Cl, Br, I). Nano Letters. 2020, 17: 460-466
https://doi.org/10.1021/acs.nanolett.6b04450

[81] Huo C, Liu X, Song X. Field-effect transistors based on van-der-waals-grown and dry-transferred all-inorganic perovskite ultrathin platelets. Journal of Physical Chemistry Letters. 2017, 8: 4785-4792
https://doi.org/10.1021/acs.jpclett.7b02028

[82] Kuang M, Wang L. Controllable Printing Droplets for High-Resolution Patterns. Advanced Materials. 2014, 26: 6950-6958
https://doi.org/10.1002/adma.201305416

[83] Ge D, Yang L, Wu G. Spray coating of superhydrophobic and angle-independent coloured films. Chemical Communications. 2014, 50: 2469-2472
https://doi.org/10.1039/c3cc48962k

[84] Gu Z, Huang Z, Li C. A general printing approach for scalable growth of perovskite single-crystal films. Science Advances. 2018, 4: 1-9
https://doi.org/10.1126/sciadv.aat2390

[85] Chouhan L, Ghimire S, Subrahmanyam C. Synthesis, optoelectronic properties and applications of halide perovskites. Chemical Society Reviews. 2020, 49: 2869-2885
https://doi.org/10.1039/C9CS00848A

[86] Chen B, Rudd PN, Yang S. Imperfections and their passivation in halide perovskite solar cells. Chemical Society Reviews. 2019, 48: 3842-3867
https://doi.org/10.1039/C8CS00853A

[87] Xu J, Buin A. Perovskite-fullerene hybrid materials suppress hysteresis in planar diodes. Nature Communications. 2015, 6: 1-8
https://doi.org/10.1038/ncomms8081

[88] Abate A, Saliba M. Supramolecular halogen bond passivation of organic-inorganic halide perovskite solar cells. Nano Letters. 2014, 14: 3247-3254 https://doi.org/10.1021/nl500627x

[89] Kavadiya S, Huang S, Niedzwiedzki DM. Under Humid Ambient Conditions. 2016, 7: 1-7 https://doi.org/10.1002/aenm.201700210

[90] Ye FY, Zhang S, Lang F, Minimizing Recombination at the Perovskite/C60 Interface through a Volatile Highly Dense Molecular Interlayer. ACS Energy Lett. 2025: 2942-2951 https://doi.org/10.1021/acsenergylett.5c00615

[91] Foley BJ, Girard J. Controlling nucleation, growth, and orientation of metal halide perovskite thin films with rationally selected additives. Journal of Materials Chemistry A. 2017, 5: 113-123 https://doi.org/10.1039/C6TA07671H

[92] Fu Y, Rea M. Selective stabilization and photophysical properties of metastable perovskite polymorphs of $CsPbI_3$ in Thin Films. Chemistry of Materials. 2017, 29: 8385-8394 https://doi.org/10.1021/acs.chemmater.7b02948

[93] Liu Z, Hu J. Chemical Reduction of Intrinsic Defects in Thicker Heterojunction Planar Perovskite Solar Cells. Advanced Materials. 2017, 29: 1-8 https://doi.org/10.1002/adma.201606774

[94] Cheng Z, Lin J. Layered organic-inorganic hybrid perovskites: Structure, optical properties, film preparation, patterning and templating engineering. CrystEngComm. 2010, 12: 2646-2662 https://doi.org/10.1039/c001929a

[95] Smith IC, Hoke ET, Solis-Ibarra D. A Layered Hybrid Perovskite Solar-Cell Absorber with Enhanced Moisture Stability. Angewandte Chemie. 2014, 126: 11414-11417 https://doi.org/10.1002/ange.201406466

[96] Jiang Q, Zhao Y. Surface passivation of perovskite film for efficient solar cells. Nature Photonics. 2019, 13: 460-466 https://doi.org/10.1038/s41566-019-0398-2

[97] Zheng X, Hou Y. Managing grains and interfaces via ligand anchoring enables 22.3%-efficiency inverted perovskite solar cells. Nature Energy. 2020, 5: 131-140 https://doi.org/10.1038/s41560-019-0538-4

[98] Zhao H, Wang S. Enhanced stability and optoelectronic properties of $MAPbI_3$ films by a cationic surface-active agent for perovskite solar cells. Journal of Materials Chemistry A. 2018, 6: 10825-10834 https://doi.org/10.1039/C8TA00457A

[99] Wang G, Wang L. Fabrication of efficient formamidinium perovskite solar cells under ambient air via intermediate-modulated crystallization. Solar Energy. 2019, 187: 147-155 https://doi.org/10.1016/j.solener.2019.05.033

[100] Binek A, Hanusch FC, Docampo P. Stabilization of the trigonal high-temperature phase of formamidinium lead iodide. Journal of Physical Chemistry Letters. 2015, 6: 1249-1253 https://doi.org/10.1021/acs.jpclett.5b00380

[101] Liang PW, Liao C. Additive enhanced crystallization of solution-processed perovskite for highly efficient planar-heterojunction solar cells. Advanced Materials. 2014, 26: 3748-3754 https://doi.org/10.1002/adma.201400231

[102] Li J, Dong X. Electronic coordination effect of the regulator on perovskite crystal growth and its high-performance solar cells. ACS Applied Materials and Interfaces. 2020, 12: 19439-19446 https://doi.org/10.1021/acsami.0c00762

[103] Bi DQ, Yi CY. Polymer-templated nucleation and crystal growth of perovskite films for solar cells with efficiency greater than 21%. Nature Energy. 2016, 1:16142 https://doi.org/10.1038/nenergy.2016.142

[104] Li G,Yao Y. 'Solvent annealing' effect in polymer solar cells based on poly(3-hexylthiophene) and methanofullerenes. Advanced Functional Materials. 2007, 17: 1636-1644 https://doi.org/10.1002/adfm.200600624

[105] Im JH, Jang IH, Pellet N, Grätzel M. Growth of CH_3 NH_3 PbI_3 cuboids with controlled size for high-efficiency perovskite solar cells. Nature Nanotechnology. 2014, 9: 927-932 https://doi.org/10.1038/nnano.2014.181

[106] Yu Y,Wang C. Synergistic Effects of Lead Thiocyanate Additive and Solvent Annealing on the Performance of Wide-Bandgap Perovskite Solar Cells. ACS Energy Letters. 2017, 2: 1177-1182 https://doi.org/10.1021/acsenergylett.7b00278

[107] Bai S, Da P. Planar perovskite solar cells with long-term stability using ionic liquid additives. Nature. 2019, 571: 245-250 https://doi.org/10.1038/s41586-019-1357-2

[108] Yang G, Qin P, Fang G. A Lewis Base-Assisted Passivation Strategy Towards Highly Efficient and Stable Perovskite Solar Cells. Solar RRL. 2018, 2: 1800055 https://doi.org/10.1002/solr.201800055

[109] Luo D, Yang W. Enhanced photovoltage for inverted planar heterojunction perovskite solar cells. Science. 2018, 360: 1442-1446 https://doi.org/10.1126/science.aap9282

[110] Zhou W, Li D. Zwitterion Coordination Induced Highly Orientational Order of $CH_3NH_3PbI_3$ Perovskite Film Delivers a High Open Circuit Voltage Exceeding 1.2 V. Advanced Functional Materials. 2019, 29: 1-11 https://doi.org/10.1002/adfm.201901026

[111] Wang Y, Ibrahim M. Thermodynamically stabilized b-CsPbI3-based perovskite solar cells with efficiencies >18%. Science. 2019, 365: 591-595 https://doi.org/10.1126/science.aav8680

[112] Peng, J. *et al*. A Universal Double-Side Passivation for High Open-Circuit Voltage in Perovskite Solar Cells: Role of Carbonyl Groups in Poly(methyl methacrylate). Advanced Energy Materials. 2018, 8:1801208 https://doi.org/10.1002/aenm.201801208

[113] Zhang Q, Zhu W. Light Processing Enables Efficient Carbon-Based, All-Inorganic Planar $CsPbIBr_2$ Solar Cells with High Photovoltages. ACS Applied Materials and Interfaces. 2019, 11: 2997-3005 https://doi.org/10.1021/acsami.8b17839

[114] Jia X, Liu L, Fang Z. TBAB additive for inorganic $CsPbI_{2.4}Br_{0.6}$ perovskite solar cells with efficiency beyond 15%. Journal of Materials Chemistry C. 2019, 7: 7207-7211 https://doi.org/10.1039/C9TC02362C

[115] Chen Q, Zhou H. Controllable self-induced passivation of hybrid lead iodide perovskites toward high performance solar cells. Nano Letters. 2014 14: 4158-4163 https://doi.org/10.1021/nl501838y

[116] Lee JW, Kim S. The Interplay between Trap Density and Hysteresis in Planar Heterojunction Perovskite Solar Cells. Nano Letters. 2017, 17: 4270-4276 https://doi.org/10.1021/acs.nanolett.7b01211

[117] Xiao M, Huang F. A fast deposition-crystallization procedure for highly efficient lead iodide perovskite thin-film solar cells. Angewandte Chemie - International Edition. 2014, 53: 9898-9903 https://doi.org/10.1002/anie.201405334

[118] Jeon NJ, Na H. A fluorene-terminated hole-transporting material for highly efficient and stable perovskite solar cells. Nature Energy. 2018, 3: 682-689 https://doi.org/10.1038/s41560-018-0200-6

[119] Liu S, Biju VP, Qi Y. Recent progress in the development of high-efficiency inverted perovskite solar cells. NPG Asia Mater. 2023, 15(1). https://doi.org/10.1038/s41427-023-00474-z

[120] Yan, P. Y.; Yang, D. B.; Wang, H. Q.; Yang, S. C.; Ge, Z. Y., Recent advances in dopant-free organic hole-transporting materials for efficient, stable and low-cost perovskite solar cells. Energy & Environmental Science 2022, 15 (9): 3630-3669. https://doi.org/10.1039/D2EE01256A

[121] Tan, Q.; Li, Z. N.; Luo, G. F.; Zhang, X. S.; Che, B.; Chen, G. C.; Gao, H.; He, D.; Ma, G. Q.; Wang, J. F.; Xiu, J. W.; Yi, H. Q.; Chen, T.; He, Z. B., Inverted perovskite solar cells using

dimethylacridine-based dopants. Nature 2023, 620 (7974): 545-551.
https://doi.org/10.1038/s41586-023-06207-0

[122] Yu, X.; Sun, X.; Zhu, Z.; Li, Z. a., Stabilization strategies of buried interface for efficient SAM based inverted perovskite solar cells. Angewandte Chemie-International Edition 2025, 64: e202419608.
https://doi.org/10.1002/anie.202419608

[123] Almasabi, K.; Zheng, X.; Turedi, B.; Alsalloum, A. Y.; Lintangpradipto, M. N.; Yin, J.; Gutiérrez-Arzaluz, L.; Kotsovos, K.; Jamal, A.; Gereige, I.; Mohammed, O. F.; Bakr, O. M., Hole-Transporting Self-Assembled Monolayer Enables Efficient Single-Crystal Perovskite Solar Cells with Enhanced Stability. ACS Energy Letters 2023, 8 (2): 950-956.
https://doi.org/10.1021/acsenergylett.2c02333

[124] Xing Z, Jin G, Du Q. Ions-induced Assembly of Perovskite Nanocomposites for Highly Efficient Light-Emitting Diodes with EQE Exceeding 30%. Adv. Mater. 2024, 36, 2406706.
https://doi.org/10.1002/adma.202406706

[125] Feng SC, Shen Y, Hu XM. Efficient and Stable Red Perovskite Light-Emitting Diodes via Thermodynamic Crystallization Control. Adv. Mater. 2024, 36, 2410255.
https://doi.org/10.1002/adma.202410255

[126] Lin K, Xiang J. Perovskite light-emitting diodes with external quantum efficiency exceeding 20 per cent. Nature. 2018, 562: 245-248
https://doi.org/10.1038/s41586-018-0575-3

[127] Kim YH, Cho H. Multicolored organic/inorganic hybrid perovskite light-emitting diodes. Advanced Materials. 2015, 27: 1248-1254
https://doi.org/10.1002/adma.201403751

[128] Tan ZK, Moghaam R. Bright light-emitting diodes based on organometal halide perovskite. Nature Nanotechnology. 2014, 9: 687-692
https://doi.org/10.1038/nnano.2014.149

[129] Longo G, Pertegás A, Martínez-Sarti L. Highly luminescent perovskite-aluminum oxide composites. Journal of Materials Chemistry C. 2015, 3: 11286-11289
https://doi.org/10.1039/C5TC02447A

[130] Zhao X, Liu T, Shi W. Capillary-written single-crystalline all-inorganic perovskite microribbon arrays for highly-sensitive and thermal-stable photodetectors. Nanoscale. 2019, 11: 2453-2459
https://doi.org/10.1039/C8NR08890J

[131] Lian Z, Yan Q. High-Performance Planar-Type Photodetector on (100) Facet of $MAPbI_3$ Single Crystal. Scientific Reports. 2015, 5: 1-10
https://doi.org/10.1038/srep16563

[132] Liu Y, Zhang Y. Thinness- and Shape-Controlled Growth for Ultrathin Single-Crystalline Perovskite Wafers for Mass Production of Superior Photoelectronic Devices. Advanced Materials. 2016, 28: 9204-9209
https://doi.org/10.1002/adma.201601995

[133] Saidaminov MI, Haque M. Inorganic Lead Halide Perovskite Single Crystals: Phase-Selective Low-Temperature Growth, Carrier Transport Properties, and Self-Powered Photodetection. Advanced Optical Materials. 2017, 5: 1600704
https://doi.org/10.1002/adom.201600704

[134] Sekizawa K, Maeda K, Domen K. Artificial Z-scheme constructed with a supramolecular metal complex and semiconductor for the photocatalytic reduction of CO_2. Journal of the American Chemical Society. 2013, 135: 4596-4599
https://doi.org/10.1021/ja311541a

[135] Abe R, Shinmei K, Hara K, Ohtani B. Robust dye-sensitized overall water splitting system with two-step photoexcitation of coumarin dyes and metal oxide semiconductors. Chemical Communications 2009,24：3577-3579
https://doi.org/10.1039/b905935k

[136] Li, F. Z.; Deng, X.; Shi, Z. S.; Wu, S. F.; Zeng, Z. X.; Wang, D.; Li, Y.; Qi, F.; Zhang, Z. M.; Yang, Z. B.; Jang, S. H.; Lin, F. R.; Tsang, S. W.; Chen, X. K.; Jen, A. K. Y., Hydrogen-bond-bridged intermediate for perovskite solar cells with enhanced efficiency and stability. Nature Photonics 2023, 17 (6), 478-484.
https://doi.org/10.1038/s41566-023-01180-6

[137] Geng, M. Q.; Li, Y. B.; Wang, Y. N.; Li, J. L.; Lu, D.; Jiang, L.; Meng, Q. Y.; Xu, T. T., Rational design of pyridine bidentate molecules for surface passivating carbon-based perovskite solar cells. Chemical Engineering Journal 2025, 510, 161648.
https://doi.org/10.1016/j.cej.2025.161648

[138] Du, S. J.; Guo, Y. X.; Wang, C.; Chen, G. Y.; Li, G.; Liang, J. W.; Chen, W. Q.; Yu, Z. Q.; Ge, Y. S.; Jia, P.; Guan, H. L.; Yu, Z. X.; Cui, H. S.; Yu, Z. H.; Ke, W. J.; Fang, G. J., Improving Crystallization of Wide-Bandgap Lead Halide Perovskite for All-perovskite Tandems. Advanced Energy Materials 2024, 202404180.
https://doi.org/10.1002/aenm.202404180

[139] Sun, M. N.; Zhang, F.; Liu, H. L.; Li, X. G.; Xiao, Y.; Wang, S. R., Tuning the crystal growth of perovskite thin-films by adding the 2-pyridylthiourea additive for highly efficient and stable solar cells prepared in ambient air. Journal of Materials Chemistry A 2017, 5 (26), 13448-13456.
https://doi.org/10.1039/C7TA00894E

[140] Zhu, H. W.; Liu, Y. H.; Eickemeyer, F. T.; Pan, L. F.; Ren, D.; Ruiz-Preciado, M. A.; Carlsen, B.; Yang, B. W.; Dong, X. F.; Wang, Z. W.; Liu, H. L.; Wang, S. R.; Zakeeruddin, S. M.; Hagfeldt, A.; Dar, M. I.; Li, X. G.; Grätzel, M., Tailored Amphiphilic Molecular Mitigators for Stable Perovskite Solar Cells with 23.5% Efficiency. Advanced Materials 2020, 32 (12), 1907757.
https://doi.org/10.1002/adma.201907757

Received on 17-04-2025 Accepted on 29-05-2025 Published on 12-06-2025

https://doi.org/10.31875/2410-2199.2025.12.05